On the Interaction between Moist Convection and Large-Scale Ascent in the Tropics

MARTIN S. SINGH[a] and SRAMANA NEOGI[a]

[a] *School of Earth, Atmosphere and Environment, Monash University, Victoria, Australia*

(Manuscript received 10 September 2021, in final form 31 January 2022)

ABSTRACT: A simple steady-state model is constructed for the interaction between moist convection and large-scale ascent in the tropics. The model is based on a bulk-plume representation of convection, and it is coupled to the large-scale circulation using methods developed for limited-area numerical models that are consistent with the weak temperature gradient approximation. Given the midtropospheric temperature anomaly in the ascent region, the model solves for the profiles of temperature, relative humidity, and large-scale vertical velocity in this region, as well as the tropical-mean profiles of temperature and relative humidity, as a function of two parameters representing the importance of entrainment and condensate re-evaporation in moist convection. According to the simple model, the ascent region is characterized by an anomalously moist and stable free troposphere with a top-heavy vertical velocity profile that peaks in the upper troposphere. These results are shown to be consistent with simulations using a cloud system–resolving model in which the large-scale circulation is parameterized. Furthermore, it is shown that, due to the effect of entrainment on the tropospheric lapse rate, the predicted vertical velocity profile is more top-heavy than the first-baroclinic mode profile used in previous reduced-complexity models of tropical dynamics. The simple model therefore provides a framework to link mixing and microphysical processes in moist convection to the large-scale structure of the tropical overturning circulation.

KEYWORDS: Atmospheric circulation; Convection; Cloud resolving models; Idealized models

1. Introduction

Understanding how moist convection influences, and is influenced by, the large-scale circulation remains a central challenge of tropical meteorology. Such understanding is a prerequisite for successful parameterization of convection within general circulation models (e.g., Arakawa and Schubert 1974). More generally, knowledge of the basic physical mechanisms that underpin the relationship between convection and the large-scale atmospheric state is crucial for interpreting observations and the results of high-resolution models and for developing theories of convectively coupled phenomena (e.g., Emanuel 2019).

In this paper, we develop a simple model for the interaction between moist convection and the large-scale circulation applicable to a region of the tropics experiencing steady ascent. Here, the phrase "large scale" refers to phenomena that vary over spatial distances of a few hundred kilometers up to the size of the planet. Our aims in constructing such a model are threefold. First, we demonstrate that the recently proposed theoretical model of tropospheric stability and humidity of Singh et al. (2019) may be coupled to the large-scale circulation in a way that respects dynamical constraints on the tropical atmosphere. Second, we show that the model is able to reproduce key aspects of cloud system–resolving model (CRM) simulations of a region of ascent in the tropics. This allows us to achieve our third and most important aim, to provide a framework linking small-scale processes within moist convection, including cloud mixing and microphysics, to the structure of the large-scale tropical overturning circulation.

Corresponding author: Martin S. Singh, martin.singh@monash.edu

Previous observational and modeling studies have highlighted important connections between convective activity and the large-scale atmospheric state. For example, it is well known that there is a strong and nonlinear relationship between precipitation and total column water vapor in the tropics (Bretherton et al. 2004), valid over both land and ocean (Schiro et al. 2016) and on a range of spatial and temporal scales (Kuo et al. 2018). At short time scales, this relationship has been interpreted as an indicator of the sensitivity of the growth of convective clouds to environmental humidity (e.g., Holloway and Neelin 2009; Ahmed and Neelin 2018). At longer time scales, the energy and moisture budgets provide additional constraints, and the moistening effects of convection itself must be taken into account (Emanuel 2019; Singh et al. 2019). Moist convection is also known to exert a strong influence on the atmosphere's thermal structure (e.g., Arakawa and Schubert 1974; Emanuel et al. 1994). A number of studies have presented evidence that tropical lapse rates tend to be smaller when the troposphere is moist and convection is widespread compared to when the troposphere is drier and the convective area fraction is lower (e.g., Singh and O'Gorman 2013; Singh et al. 2017; Davies et al. 2013; Gjorgjievska and Raymond 2014; Raymond et al. 2015).

Singh et al. (2019) developed a simple steady-state model to help explain the above relationships based on the assumptions that convection acts to drive the atmosphere toward a state that is neutrally buoyant with respect to an entraining plume (Singh and O'Gorman 2013) and that the environmental humidity is determined through a balance between moistening by convective detrainment and drying by subsidence (Romps 2014). This zero-buoyancy plume (ZBP) model was able to provide a mechanistic explanation for the relationships between precipitation, humidity, and instability across simulations with a CRM in which a steady large-scale flow

DOI: 10.1175/JCLI-D-21-0717.1

was imposed. However, as pointed out by Romps (2021), the model fails to take into account the tendency for gravity waves to homogenize the virtual temperature profile within the tropics, and, when applied to explain tropical variability, it predicts horizontal temperature gradients much larger than those observed. Here, we address this criticism by coupling the model of Singh et al. (2019) to the large-scale circulation using methods developed for simulating the tropical atmosphere in limited-area numerical models, namely the weak temperature gradient (WTG; Sobel and Bretherton 2000) and damped gravity wave (DGW; Kuang 2008a) parameterizations. The resultant coupled zero-buoyancy plume (CZBP) model explicitly takes into account dynamic constraints on the atmospheric thermal structure; as a result, it allows the free-tropospheric temperature within the ascent region to remain close to that of the tropical mean, satisfying the weak temperature gradient approximation. At the same time, consistent with the results of Singh et al. (2019) and Warren et al. (2020), we find that the ascent region has a moister and more stable troposphere than that of the tropical mean state.

Extending the ZBP model of Singh et al. (2019) to include dynamic constraints has the added benefit of incorporating the structure of the circulation into the model solution. Specifically, the model predicts the vertical profile of vertical velocity averaged over the ascent region as a function of parameters representing the strength of mixing and re-evaporation processes within moist convection. In the tropics, the shape of the vertical velocity profile is a key determinant of the energy transport associated with large-scale overturning circulations through its effect on the gross moist stability (Neelin and Held 1987).

Theories for the gross moist stability and the vertical structure of the tropical overturning circulation commonly consider a representation of the vertical velocity that comprises a small number of modal structure functions. For example, Neelin and Zeng (2000) showed that the assumption of convective quasi-equilibrium (QE), in which the tropospheric lapse rate is assumed to remain nearly equal to that of a moist adiabat, constrains tropical overturning circulations to conform to a single "first-baroclinic mode" vertical structure, in which the vertical velocity profile peaks in the upper troposphere. The resultant theoretical framework, known as QE dynamics (Emanuel 2007), and the associated numerical model, known as the quasi-equilibrium tropical circulation model (Neelin and Zeng 2000; Zeng et al. 2000), have provided a range of insights into the behavior of tropical circulations and their response to changes in climate (e.g., Chou and Neelin 2004; Neelin 2007; Levine and Boos 2016).

However, other studies have highlighted the need for at least two modes of the vertical velocity, with maxima in the upper and lower troposphere, respectively, to adequately account for the range of circulations observed in the tropics (e.g., Back and Bretherton 2006, 2009a,b; Duffy et al. 2020). The relative importance of each mode affects the level at which the vertical velocity maximizes and, in doing so, controls the gross moist stability. Kuang (2011) used such a two-mode decomposition to develop a theory for the dependence of the gross moist stability on the wavelength of the associated circulation. He found that the gross moist stability decreases with wavelength, potentially providing a scale-selection mechanism for certain types of planetary-scale tropical disturbances.

While the CZBP model developed here solves for the full vertical velocity profile without decomposition into modes, the dynamics remain truncated through the use of simplified approximations in the methods of coupling. Nevertheless, we show that the dynamical structures predicted by the CZBP model compare well to those obtained in simulations performed with a CRM in which the large-scale circulation is parameterized using similar WTG and DGW coupling methods. This provides confidence that the CZBP model is able to reproduce key aspects of the convective response. We further show that the first-baroclinic mode structure of QE dynamics is obtained for a limiting case of the CZBP model in which mixing between the clouds and their environment is negligible and does not affect the lapse rate of the ascent region or of the tropical mean state. According to the CZBP model, the effect of mixing is to enhance ascent in the upper troposphere relative to that in the lower troposphere, implying a larger gross moist stability. The CZBP model therefore enables one to relate details of convective-scale dynamics to large-scale properties of the flow.

The rest of the paper is organized as follows. We first derive the CZBP model and describe the method used to solve it (section 2). We then document the basic dynamic and thermodynamic properties of the solution (section 3), and we compare the results to those obtained in CRM simulations in which the large-scale circulation is parameterized (section 4). Finally, we present a summary and discussion (section 5).

2. Coupled zero-buoyancy plume model

We construct a simple steady-state model for the dynamic and thermodynamic structure of the atmosphere in a region of large-scale ascent. We solve for the average profiles of temperature $T(z)$, relative humidity $\mathcal{R}(z)$, and vertical velocity $w(z)$ in the ascent region as a function of height z. The background profiles of temperature $T_0(z)$ and relative humidity $\mathcal{R}_0(z)$, representing the tropical mean state, are taken as the solution under radiative-convective equilibrium (RCE) conditions, for which $w(z) = 0$.

The model is made up of two components: a thermodynamic model and a dynamic model. The thermodynamic model solves for the steady-state thermodynamic structure of the atmosphere under the influence of a given large-scale vertical velocity profile (section 2a). The dynamic model diagnoses the large-scale vertical velocity $w(z)$ from the temperature anomaly in the ascent region $\Delta T(z) = T - T_0$ (section 2b). By iteratively coupling these two models together, we are able to solve for the steady-state thermodynamic and dynamic structures of the ascent region given the value of the temperature anomaly $\Delta T_{\mathrm{ref}} = \Delta T(z_{\mathrm{ref}})$ at a single level z_{ref} and two parameters that are related to the importance of entrainment and condensate re-evaporation within moist convection (section 2c). We refer to this coupled model as the coupled zero-buoyancy plume (CZBP) model, although the ZBP approximation is only applied within its thermodynamic component.

a. Thermodynamic model

The thermodynamic model solves for the temperature and relative humidity profiles of the atmosphere given the large-scale vertical velocity profile. It is based on the ZBP approximation, introduced by Bretherton and Park (2008) and Singh and O'Gorman (2013) for shallow and deep convection, respectively, and used in Romps (2014, 2021), Singh and O'Gorman (2015), and Singh et al. (2019). According to the ZBP approximation, convection constrains the tropospheric density profile such that it remains neutrally buoyant with respect to an entraining plume. Owing to the influence of entrainment, the tropospheric lapse rate is then dependent on the relative humidity of the cloud environment. Following Romps (2014), we determine the environmental relative humidity by assuming a steady-state balance between moistening of the environment by detrainment of water vapor and condensate from clouds and drying of the environment by subsidence.

Singh et al. (2019) used the above assumptions to solve for the temperature and relative humidity profiles of the atmosphere given the upward mass flux in convection and the downward mass flux in the environment. Romps (2021) derived an analytic solution for the lapse rate, relative humidity, and convective mass flux as a function of the net vertical mass flux ρw under the additional assumptions that detrainment of cloud water and the variation of the convective mass flux with height may be neglected.[1] Here, we extend the analytic solution of Romps (2021) to include a crude representation of condensate detrainment, and we apply it to provide a complete numerical solution for the thermodynamic structure of the atmosphere under large-scale ascent.

Within the troposphere, the thermodynamic model represents convection as a steady-state bulk entraining plume. The model domain is divided into a saturated convective region with a mass flux $M_c(z)$ and an unsaturated environment with a mass flux $M_e(z)$. On physical grounds, and recently confirmed observationally by Yin et al. (2021), we expect the environmental mass flux to be downward. Defining upward mass fluxes to be positive, we therefore expect $M_e(z)$ to be negative. The net upward mass flux over the domain ρw is then given by

$$\rho w = M_c + M_e. \tag{1}$$

Note that we express all mass fluxes per unit area of the domain.

For the simple case of radiative-convective equilibrium (RCE), the vertical velocity $w(z)$ is zero, and subsidence in the environment balances ascent within convection. When $w(z) \neq 0$, mass continuity requires there to be a horizontal convergence of mass $l(z)$ to balance the vertical mass divergence associated with the vertical velocity:

$$l(z) = \frac{\partial(\rho w)}{\partial z}. \tag{2}$$

Following Romps (2021), we describe the thermodynamic model in terms of specific humidity and moist static energy. We define q to be the environmental specific humidity and h to be the environmental moist static energy. Neglecting virtual effects, the ZBP assumption states that the temperatures of the environment and the convective region are equal to the domain-mean temperature T. Further neglecting the effects of water on the specific heat capacity, we may write the environmental moist static energy as

$$h = c_p T + gz + L_v q, \tag{3}$$

where c_p is the isobaric specific heat capacity, g is the gravitational acceleration, and L_v is the latent heat of vaporization. The humidity and moist static energy of the convective region are then given by q^* and h^*, respectively, where an asterisk refers to a variable at saturation. With these definitions, we may write down the governing equations for the thermodynamic model:

$$\frac{\partial M_c}{\partial z} = e - d, \tag{4a}$$

$$\frac{\partial M_e}{\partial z} = d - e + l, \tag{4b}$$

$$\frac{\partial (M_c q^*)}{\partial z} = eq - dq^* - s_{\text{cond}}, \tag{4c}$$

$$\frac{\partial (M_e q)}{\partial z} = dq^* - eq + lq + s_{\text{evap}}, \tag{4d}$$

$$\frac{\partial (M_c h^*)}{\partial z} = eh - dh^*, \tag{4e}$$

$$\frac{\partial (M_e h)}{\partial z} = dh^* - eh + lh + Q_{\text{rad}}, \tag{4f}$$

$$h^* - h = q^* - q. \tag{4g}$$

Here, e is the rate of entrainment of mass from the environment into the convective region, d is the rate of detrainment of mass from the convective region into the environment, s_{cond} represents the sink of water vapor within the convective region due to condensation, s_{evap} represents the source of water vapor within the environment due to evaporation of condensate that has been detrained from convection, and Q_{rad} gives the radiative heating rate, all expressed per unit volume. The final equation expresses the ZBP approximation of equal temperature in the convective region and the environment. We have further assumed that the specific humidity and moist static energy of the air surrounding the model domain are equal to that of the environment, and this has allowed us to neglect horizontal advection of those two variables. Additionally, we have assumed that the area fraction of convection is sufficiently small that we may neglect radiative heating within the convective region and we may assume that the mass convergence $l(z)$ occurs exclusively into the

[1] Singh et al. (2019) also presented an analytic solution for the precipitation rate as a function of relative humidity under additional assumptions, but, as shown by Romps (2021), these assumptions result in an inconsistency in the model. This inconsistency affects Fig. 2 of Singh et al. (2019), but all other results in that work are consistent with the thermodynamic model derived here.

environment. Note that the radiative effects of clouds may still be included through the effect of detrained clouds on the radiative heating of the environment Q_{rad}.

For given values of entrainment e, detrainment d, large-scale convergence l, and radiative cooling Q_{rad}, the equation set (4a)–(4g) represents seven equations in the eight unknowns M_c, M_e, q, q^*, h, h^*, s_{cond}, and s_{evap}. The equation set may therefore be solved given a parameterization for the evaporation rate s_{evap}. For example, Romps (2021) solved this set for the simple case $s_{\text{evap}} = 0$. Here we instead follow Singh et al. (2019) and apply a crude parameterization of evaporation given by

$$s_{\text{evap}} = \mu d(q^* - q), \tag{5}$$

where μ is a nondimensional constant measuring the importance of condensate evaporation in moistening the environment. As pointed out by Singh et al. (2019), (5) cannot be justified rigorously, but it has the useful properties that s_{evap} increases with the rate of detrainment of mass from clouds and decreases to zero as the environment approaches saturation.

Defining the fractional entrainment rate $\epsilon = e/M_c$ and the fractional detrainment rate $\delta = d/M_c$, and approximating the relative humidity as $\mathcal{R} = q/q^*$, we may use (4a) and (4b) to rearrange (4c)–(4f) to give the following:

$$M_c \frac{\partial q^*}{\partial z} = -\epsilon(1-\mathcal{R})M_c q^* - s_{\text{cond}}, \tag{6a}$$

$$M_e \frac{\partial q}{\partial z} = \delta(1+\mu)(1-\mathcal{R})M_c q^*, \tag{6b}$$

$$M_c \frac{\partial h^*}{\partial z} = -\epsilon L_v(1-\mathcal{R})M_c q^*, \tag{6c}$$

$$M_e \frac{\partial h}{\partial z} = \delta L_v(1-\mathcal{R})M_c q^* + Q_{\text{rad}}, \tag{6d}$$

where we have used the ZBP assumption (4g) to write $h^* - h = L_v(1-\mathcal{R})q^*$.

Following Singh et al. (2019), the equation set above may be used to derive expressions for the relative humidity $\mathcal{R}$ and the temperature lapse rate $\Gamma = -\partial_z T$. By approximating $\partial_z q = \mathcal{R}\partial_z q^*$, (6b) may be written as

$$\mathcal{R} = \frac{\delta(1+\mu)}{\delta(1+\mu) + r\gamma}, \tag{7}$$

where $r = -M_e/M_c$ and $\gamma = -\partial_z \ln(q^*)$. Noting that $q^* = q^*(T, p)$ is a thermodynamic function of temperature and pressure, we may use the chain rule and hydrostatic balance to write γ in terms of the temperature lapse rate Γ (Romps 2014):

$$\gamma = \frac{L_v\Gamma}{R_v T^2} - \frac{g}{R_d T}. \tag{8}$$

Here R_d and R_v are the gas constants for dry air and water vapor, respectively, and we have neglected virtual effects.

To derive an equation for the temperature lapse rate Γ, we differentiate the definition of the saturation moist static energy to give

$$\frac{\partial h^*}{\partial z} = -c_p\Gamma + g - L_v\gamma q^*. \tag{9}$$

Substituting this expression into (6c) and using (8) gives, with some rearrangement,

$$\Gamma = \Gamma_m + \frac{\epsilon L_v q^*(1-\mathcal{R})}{c_p + \dfrac{q^* L_v^2}{R_v T^2}}, \tag{10}$$

where

$$\Gamma_m = \left(\frac{g}{c_p}\right)\frac{1 + \dfrac{q^* L_v}{R_d T}}{1 + \dfrac{q^* L_v^2}{c_p R_v T^2}} \tag{11}$$

is the moist adiabatic lapse rate.

Equations (7) and (10) give the essence of the thermodynamic model. As the net mass flux ρw increases, we expect the upward mass flux in convection to increase relative to the downward mass flux in the environment, resulting in a decrease in the magnitude of r. According to (7), for a fixed detrainment rate δ and evaporation parameter μ, this leads to an increase in relative humidity. According to (10), for a fixed positive entrainment rate ϵ, the troposphere becomes increasingly stable (smaller Γ) with increasing relative humidity, and the lapse rate approaches that of a moist adiabat as the troposphere approaches saturation $\mathcal{R} \to 1$. Taken together, these results suggest that the troposphere becomes moister and more stable under large-scale ascent. However, the model is not yet complete because we have not established a quantitative expression for r in terms of the vertical velocity w. The full solution is derived in appendix A using a method adopted from Romps (2021). Specifically, we use (6a)–(6d) and (1) to find closed expressions for the relative humidity $\mathcal{R}$ and temperature lapse rate $\Gamma = -\partial_z T$ as a function of the vertical velocity w, given the radiative heating rate Q_{rad}, temperature T, pressure p, entrainment rate ϵ, detrainment rate δ, and evaporation parameter μ. The lapse rate is then integrated vertically, in combination with the equation for hydrostatic balance, to provide a complete thermodynamic profile given the temperature and pressure at a single level. In performing such an integration, the entrainment and detrainment rates should, in principle, be related via (4a), which may be written as

$$\frac{\partial \ln M_c}{\partial z} = \epsilon - \delta. \tag{12}$$

For simplicity, here we follow Romps (2021) and neglect the variation of the convective mass flux with height, so that $\epsilon = \delta$ at all heights. We test the range of validity of this approximation a posteriori.

The thermodynamic model requires as an input the radiative heating rate Q_{rad}. Based on the observation that the clear-sky cooling rate of the tropical atmosphere is strongly constrained by the temperature dependence of the saturation humidity (Hartmann et al. 2001), we specify Q_{rad} to be a function of temperature T as follows:

$$-\frac{Q_{\rm rad}}{\rho c_p} = \begin{cases} K, & T \geq T_m, \\ K\left[\frac{1}{2} + \frac{1}{2}\cos\left(\pi \frac{T_m - T}{T_m - T_t}\right)\right], & T_t < T < T_m, \\ 0, & T \leq T_t. \end{cases} \quad (13)$$

Here the left-hand side gives the negative temperature tendency due to radiation in units of kelvin per unit time. The negative temperature tendency is constant at a value $K = 1$ K day^{-1} in the lower troposphere, begins to decrease in magnitude in the midtroposphere at the temperature $T_m = 250$ K, and reaches zero at the tropopause temperature $T_t = 200$ K (Fig. 1). These parameters are set to roughly match the mean radiative cooling profile of a CRM simulation of RCE described in section 4. Note that this simple parameterization neglects changes in the radiative cooling rate associated with changes in the large-scale circulation. While we expect circulation-induced changes in the cloud and water vapor distribution to be important in setting $Q_{\rm rad}$, the resultant effect on the circulation is likely to be a secondary effect.

Upon specification of the entrainment rate ϵ, evaporation parameter μ and the temperature $T_{\rm ref}$ and pressure $p_{\rm ref}$ at a reference height $z_{\rm ref}$, appendix A shows how the thermodynamic model may be used to find the temperature and relative humidity profiles of the atmosphere for a given vertical velocity profile $w(z)$. Within the troposphere, the relative humidity is calculated from (A11) and the temperature is determined by integrating (10) vertically. Within the boundary layer, at levels below $z_b = 500$ m, the lapse rate is assumed to be dry adiabatic, while above the tropopause, defined as the level at which $T = T_t$, the atmosphere is assumed to be isothermal. The relative humidity is only specified within the troposphere.

b. Dynamic model

Due to the small value of the Coriolis parameter near the equator, horizontal density gradients within tropical regions imply large balanced velocities. As a result, such density gradients are weak in the tropics compared to higher latitudes (Charney 1963). This observation has led a number of studies to propose parameterizations of the large-scale circulation suitable for limited-area numerical models that explicitly relate the domain-averaged vertical velocity to a measure of buoyancy calculated relative to a background thermodynamic profile (e.g., Sobel and Bretherton 2000; Raymond and Zeng 2005; Kuang 2008a). Based on these studies, we define the dynamic model as an expression for the vertical velocity profile $w(z)$ of the form

$$w(z) = \mathcal{L}(T - T_0), \quad (14)$$

where $\mathcal{L}$ is a linear operator. While virtual effects are quantitatively important for assessing buoyancy anomalies in the tropical atmosphere (Bao and Stevens 2021), for simplicity, our dynamic model neglects such effects and is based on the temperature anomaly in the ascent region relative to the background state given by $\Delta T(z) = T - T_0$.

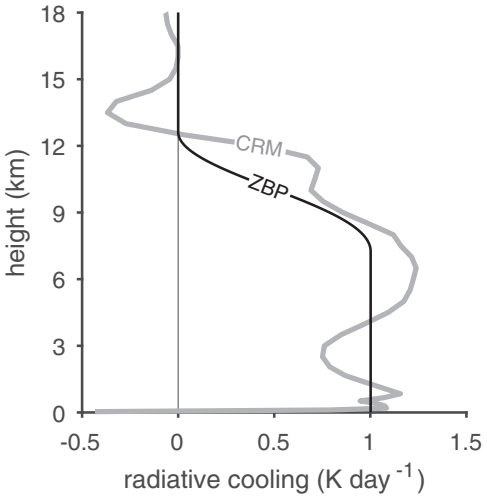

FIG. 1. Profile of radiative cooling $-Q_{\rm rad}/\rho c_p$ in RCE according to the CZBP model (black) and in the CRM simulation (gray). The CZBP profile given by (13) is evaluated using the temperature profile shown in Fig. 3a. The simulated profile is taken as the horizontal and time mean over days 50–100.

Two separate methods have been developed to parameterize the vertical velocity via (14). The first, known as the weak temperature gradient (WTG) parameterization, assumes that the large-scale circulation acts to relax the atmosphere toward the background temperature profile $T_0(z)$ (Sobel and Bretherton 2000; Raymond and Zeng 2005; Wang and Sobel 2011). The second, known as the damped gravity wave (DGW) parameterization, considers the interaction between convection and a gravity wave with a single horizontal wavenumber (Kuang 2008a; Romps 2012a). Studies using CRMs have shown that these methods result in substantially different vertical velocity profiles even under identical forcing (Daleu et al. 2015, 2016; Romps 2012b). Here we will apply both methods, and we will show that the CZBP model is able to reproduce some of the main differences in the vertical velocity profiles produced by the DGW and WTG parameterizations when applied to a CRM.

1) WEAK-TEMPERATURE GRADIENT PARAMETERIZATION

The WTG parameterization assumes that the temperature tendency owing to vertical advection relaxes the atmosphere toward the tropical-mean background temperature profile. Specifically, the vertical velocity is diagnosed via

$$-w(z)\max[\Gamma_d - \Gamma, \Gamma_{\rm min}] = -\frac{T - T_0}{\tau_{\rm WTG}}, \quad (15)$$

where $\Gamma = -\partial_z T$ is the lapse rate, $\Gamma_d = g/c_p$ is the dry-adiabatic lapse rate, and $\tau_{\rm WTG}(z)$ is a height-dependent relaxation time scale. To prevent unrealistically large diagnosed vertical velocities, we set $\Gamma_{\rm min} = 1$ K km^{-1} following Raymond and Zeng (2005) and Wang and Sobel (2011).

Equation (15) is valid in the free troposphere, where gravity waves efficiently remove buoyancy anomalies. We therefore

apply (15) between the top of the boundary layer $z_b = 500$ m and the tropopause z_t, given by the height at which the temperature $T = T_t$. Below z_b the vertical velocity is interpolated linearly in height from its value at z_b to zero at the surface, while above z_t the vertical velocity is assumed to be zero. We further set the time scale of relaxation $\tau_{\rm WTG}(z)$ to be large near z_b and z_t and smallest in the midtroposphere. Specifically, we define

$$\tau_{\rm WTG}(z) = \frac{\tau_{\rm WTG}^{\rm min}}{\sin\left(\pi \dfrac{z - z_b}{z_t - z_b}\right)}, \tag{16}$$

with the minimum value of the relaxation time scale $\tau_{\rm WTG}^{\rm min} = 3$ h. Raymond and Zeng (2005) and Sessions et al. (2010) used a similar vertical profile of $\tau_{\rm WTG}(z)$ to apply the WTG method to CRM simulations. Combining (15) and (16), we may write an expression for the vertical velocity as follows:

$$w(z) = \sin\left(\pi \frac{z - z_b}{z_t - z_b}\right) \frac{T - T_0}{\tau_{\rm WTG}^{\rm min} \max[\Gamma_d - \Gamma, \Gamma_{\rm min}]}, \tag{17}$$

which defines the dynamic model under the WTG parameterization.

2) Damped gravity wave parameterization

A disadvantage of the WTG parameterization is that it does not explicitly invoke the momentum equation in determining $w(z)$. An alternate approach, introduced by Kuang (2008a), is to consider the interaction between moist convection within a column of the atmosphere and a large-scale gravity wave with a single horizontal wavenumber k. Starting with a linearized version of the anelastic momentum equation, Kuang (2008a) showed that the large-scale vertical velocity profile at a given location satisfies

$$\frac{\partial}{\partial z}\left[\left(\frac{\partial}{\partial t} + \frac{1}{\tau_{\rm DGW}}\right)\frac{\partial(\rho w)}{\partial z}\right] = -k^2 \rho g \frac{T_v - T_{v0}}{T_{v0}}, \tag{18}$$

where $\tau_{\rm DGW}$ is a damping time scale, $\rho(z)$ and $T_v(z)$ are the density and virtual temperature profiles of the given column, respectively, and $T_{v0}(z)$ is a background virtual temperature profile. In our dynamic model, we consider the steady-state limit, neglect virtual effects, and assume $\tau_{\rm DGW}$ is independent of height so that the vertical velocity satisfies

$$\frac{\partial^2(\rho w)}{\partial z^2} = -(\tau_{\rm DGW} k^2 \rho g)\frac{T - T_0}{T_0}, \tag{19}$$

where $\rho(z)$ is the density profile of the ascent region. We follow Wang et al. (2013) and Daleu et al. (2015, 2016) to set $\tau_{\rm DGW} = 24$ h and $k = 10^{-6}$ m^{-1}. The dynamic model under the DGW parameterization is obtained by solving (19) numerically using Thomas's algorithm with the boundary conditions that $w = 0$ at $z = 0$ and $z = z_t$.

c. Coupling

We may describe the thermodynamic model derived above as a function $\mathcal{T}$ that gives the temperature and relative humidity profiles as outputs and takes the vertical velocity profile $w(z)$ and a set of parameters as inputs:

$$[T(z), \mathcal{R}(z)] = \mathcal{T}[w(z), \epsilon, \mu, T_{\rm ref}, p_{\rm ref}, z_{\rm ref}]. \tag{20}$$

Similarly, we may describe the dynamic model as a function $\mathcal{W}$ that gives the vertical velocity profile as an output and takes the temperature profile $T(z)$ and a background temperature profile $T_0(z)$ as inputs:

$$[w(z)] = \mathcal{W}[T(z), T_0(z)]. \tag{21}$$

The precise form of $\mathcal{W}$ depends on whether one implements the WTG or DGW parameterization.

To couple the thermodynamic and dynamic models together, we first calculate the background profiles of temperature $T_0(z)$ and relative humidity $\mathcal{R}_0(z)$. Since these profiles represent the tropical mean state, we define them as the solution of the thermodynamic model under RCE conditions. That is, we set

$$[T_0(z), \mathcal{R}_0(z)] = \mathcal{T}[w_0(z); \epsilon, \mu, T_{\rm ref}, p_{\rm ref}, z_{\rm ref}], \tag{22}$$

where $w_0(z) = 0$. For this calculation, we choose a midtropospheric value of $z_{\rm ref} = 8$ km, and we set $T_{\rm ref}$ and $p_{\rm ref}$ to match the mean temperature and pressure at 8 km from a CRM simulation of RCE described in section 4. We further set the parameters $\epsilon = 0.6$ km^{-1} and $\mu = 1.5$ in order to provide a good fit to the mean temperature and relative humidity profiles of this RCE simulation. This fitting procedure is described in appendix B. Having matched the theoretical RCE solution to the time-mean profiles from a CRM simulation, we hold these parameters fixed in the calculations to follow (Table 1).

To calculate the temperature and relative humidity profiles in the ascent region, we calculate new profiles $T_1(z)$ and $\mathcal{R}_1(z)$ by applying the thermodynamic model to a reference state with a positive temperature anomaly $\Delta T_{\rm ref}$,

$$[T_1(z), \mathcal{R}_1(z)] = \mathcal{T}[w_0(z); \varepsilon, \mu, T_{\rm ref} + \Delta T_{\rm ref}, p_{\rm ref}, z_{\rm ref}].$$

This allows the dynamic model to be used to calculate a new vertical velocity profile $w_1(z)$ given by

$$[w_1(z)] = \mathcal{W}[T_1(z), T_0(z)]. \tag{23}$$

However, the vertical velocity $w_1(z)$ is not consistent with the thermodynamic profiles $T_1(z)$ and $\mathcal{R}_1(z)$, since the thermodynamic profiles were calculated assuming zero vertical velocity. We therefore conduct an iteration procedure whereby the profiles at step i are calculated from the vertical velocity profile at step $i - 1$ via

$$[T_i(z), \mathcal{R}_i(z)] = \mathcal{T}[w_{i-1}(z); \epsilon, \mu, T_{\rm ref} + \Delta T_{\rm ref}, p_{\rm ref}, z_{\rm ref}],$$
$$[w_i(z)] = c\mathcal{W}[T_i(z), T_0(z)] + (1 - c)w_{i-1}(z),$$

and the process is repeated until the vertical velocity profile converges. Here the parameter c is introduced to stabilize the iteration. We find $c = 0.4$ provides a convergent solution for all cases we tested. Here, we set the criterion for

TABLE 1. Parameters used in the solution of the CZBP model.

Parameter		Value
Depth of boundary layer	z_b	500 m
Thermodynamic model		
Entrainment rate	ϵ	0.6 km^{-1}
Evaporation parameter	μ	1.5
Reference height	$z_{\rm ref}$	8.0 km
Reference temperature	$T_{\rm ref}$	243.8 K
Reference pressure	$p_{\rm ref}$	370 hPa
Radiation parameters		
Radiative cooling rate	K	1.0 K day^{-1}
Midtropospheric temperature	T_m	250 K
Tropopause temperature	T_t	200 K
Dynamic model		
Tropopause height	z_t	Height where $T = T_t$
WTG parameterization		
Minimum relaxation time scale	$\tau_{\rm WTG}^{\rm min}$	3.0 h
Minimum lapse rate	$\Gamma_{\rm min}$	1.0 K km^{-1}
DGW parameterization		
Wavenumber	k	10^{-6} m^{-1}
Damping time scale	$\tau_{\rm DGW}$	24 h

convergence to be when $|w_i(z) - w_{i-1}(z)| < 1 \times 10^{-9}$ m s^{-1} at all levels.

As mentioned previously, we choose $z_{\rm ref} = 8$ km so that $\Delta T_{\rm ref}$ represents a temperature anomaly in the midtroposphere. This is motivated by the solutions themselves, which show a direct relationship between the temperature anomaly in the mid troposphere and the strength of the resulting large-scale ascent. We discuss the sensitivity of the CZBP model to this choice in the next section.

The procedure above describes the complete solution of the CZBP model, and it is summarized schematically in Fig. 2. Note that, even once convergence has been achieved, the solution remains inconsistent because of our assumption that $\epsilon = \delta$ throughout the troposphere. In principle, one could take ϵ as fixed and recalculate δ at each iteration to satisfy (12). However, it is practically difficult to achieve convergence in this case because (12) connects the detrainment rate to the vertical derivative of the mass flux. We therefore retain the approximation $\epsilon = \delta$, which is valid provided the vertical variation of the mass flux with height remains small, and we leave incorporation of a height-dependent detrainment rate to future work.

3. Results

a. Background (RCE) state

Figure 3 shows the background thermodynamic profiles according to the CZBP model, given by the RCE solution for which $w(z) = 0$. The temperature profile $T_0(z)$ decreases with height from the surface up to the tropopause, above which the stratosphere is assumed to be isothermal. Due to the effect of entrainment, the lapse rate within the troposphere is larger than that of a moist adiabat, implying nonzero convective available potential energy (Singh and O'Gorman 2013; Seeley and Romps 2015).

The background relative humidity profile $\mathcal{R}_0(z)$ also monotonically decreases with height from a maximum of roughly 0.9 at the top of the boundary layer to 0.5 at the tropopause (Fig. 3b). This contrasts with the C-shaped relative humidity profile, with a minimum in the midtroposphere and maxima near the boundary layer and the tropopause, found by Romps (2014) using a similar model of RCE based on the ZBP assumption. The reason for this discrepancy is that here we have neglected the variation of the convective mass flux with height by setting $\epsilon = \delta$. Romps (2014), on the other hand, assumes a fixed fractional entrainment rate but allows the detrainment rate to vary in order to satisfy (12). This implies that, as the convective mass flux decreases toward zero near the tropopause, the fractional detrainment rate increases toward infinity and the relative humidity approaches one. Therefore, the assumptions of an invariant convective mass flux and a constant fractional detrainment rate are invalid at levels near the tropopause, and our CZBP solution for the relative humidity becomes inaccurate at those levels. In

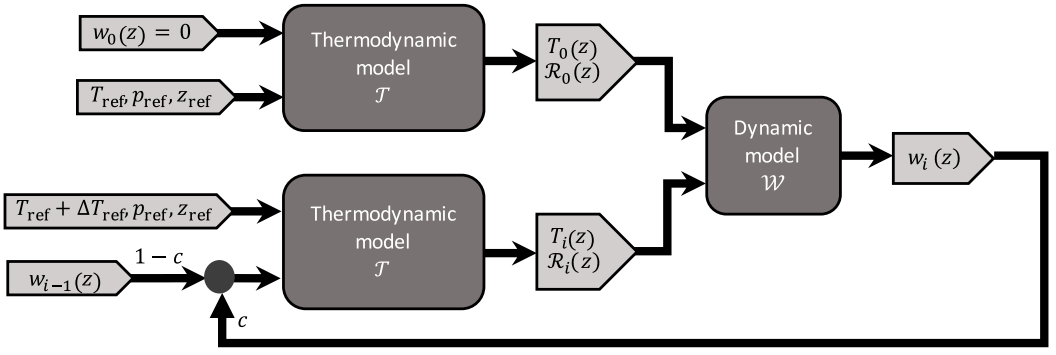

FIG. 2. Schematic representation of the iterative solution of the CZBP model. The upper branch shows the calculation of the RCE background state, representing the tropical-mean thermodynamic profiles, while the lower branch shows the calculation of the thermodynamic profiles in the ascent region based on the vertical velocity profile from the previous iteration. The two branches are then input to the dynamic model to calculate a new vertical velocity profile, which is then used as input for the next iteration.

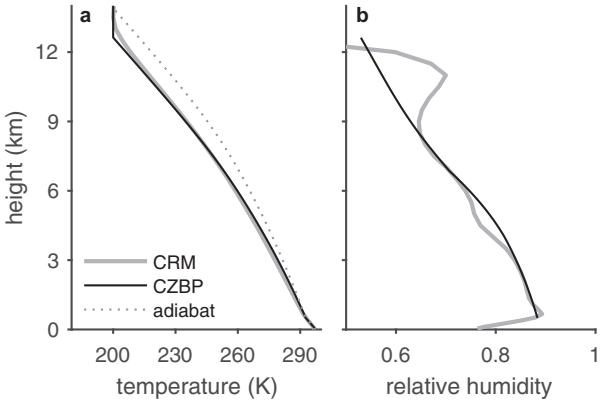

FIG. 3. (a) Temperature and (b) relative humidity profiles in RCE according to the CZBP model (black) and in CRM simulation (gray). Simulated profiles are taken as the horizontal and time mean over days 50–100. The dotted line in (a) gives the moist adiabat calculated by integrating the CZBP model upward from the level $z_b = 500$ m with the entrainment rate set to zero.

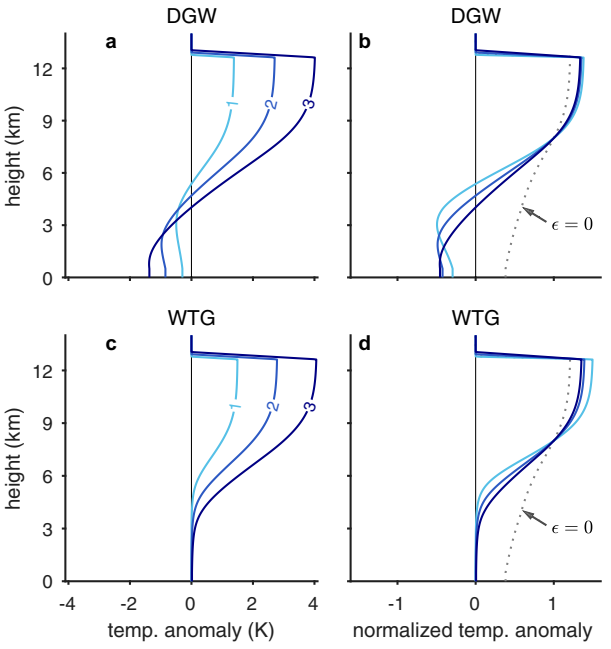

FIG. 4. Profiles of (a),(c) temperature anomalies $\Delta T(z)$ and (b),(d) temperature anomalies normalized by the reference temperature anomaly $\Delta T/\Delta T_{\rm ref}$ according to the CZBP model under the (top) DGW and (bottom) WTG parameterizations. Colors represent values of $\Delta T_{\rm ref}$ of 1, 2, and 3 K as labeled in (a) and (c). Dotted lines in (b) and (d) give results for the solution of the CZBP model with the entrainment rate $\epsilon = 0$.

principle, this inaccuracy may affect the temperature at all levels through the iteration procedure and the elliptic operator in the DGW parameterization. However, since the effect of entrainment on the lapse rate is proportional to the absolute humidity deficit, and since the saturation humidity at levels near the tropopause is orders of magnitude smaller than in the lower troposphere, the effect on the temperature profile is likely to be negligible (see also section 3c below).

b. *Structure of the ascent region*

We now consider the solution for the ascent region. We solve the CZBP model for positive temperature anomalies $\Delta T_{\rm ref} = 1$, 2, and 3 K at a height $z_{\rm ref} = 8$ km using the DGW and WTG dynamic models. In all cases, the temperature anomaly profile $\Delta T(z)$ increases with height through most of the troposphere, reaching a maximum just below the tropopause (Figs. 4a,c). For the DGW solutions, this leads to negative values $\Delta T(z) < 0$ in the boundary layer and lower troposphere, whereas in the WTG solutions the temperature anomaly remains positive but becomes negligible in the boundary layer and lower troposphere. The change in sign of $\Delta T(z)$ with height in the DGW solutions is a particularly surprising feature of the CZBP model, and it implies that the boundary layer of the ascent region is colder than that of the tropical mean. A further important characteristic of the CZBP model is that it is nonlinear. The profiles of $\Delta T(z)$ do not simply scale with the imposed anomaly $\Delta T_{\rm ref}$; rather, as $\Delta T_{\rm ref}$ becomes larger, the shape of the profile changes so that the normalized temperature anomaly $\Delta T(z)/\Delta T_{\rm ref}$ increases in the lower troposphere and decreases in the upper troposphere (Figs. 4b,d).

To understand the above results, we consider the factors controlling the lapse rate within the CZBP model. A profile of $\Delta T(z)$ that increases with height indicates that the ascending region has a lower lapse rate (is more stable) than the tropical-mean background state. In the CZBP model solutions, this lapse rate variation is primarily a result of convective entrainment. This may be seen by considering the model for the case of zero entrainment ($\epsilon = 0$; dotted lines on Figs. 4b,d). In this case, entrainment plays no role in setting the lapse rate of the ascent region *or* the tropical-mean background state, and the relative humidity becomes immaterial to the solution [formally, (7) simplifies to $\mathcal{R} = 0$ in this case]. The $\epsilon = 0$ case therefore corresponds to the assumption of moist adiabatic lapse rates in the troposphere. Under this assumption, the temperature dependence of the moist-adiabatic lapse rate leads to a profile of $\Delta T(z)$ that increases with height (see also Yu and Neelin 1997), but the increase is much weaker than for the solutions that include entrainment. Additionally, when entrainment is set to zero, the shape of the $\Delta T(z)$ profile is independent of the dynamic model and virtually independent of $\Delta T_{\rm ref}$ (for this reason only a single $\epsilon = 0$ solution is plotted in Figs. 4b and 4d).

When entrainment is included in the CZBP model, the lapse rate becomes larger (less stable) than that of a moist adiabat by an amount that increases with decreasing relative humidity. It is important to note that entrainment affects the lapse rate of both the ascent region and background state, but the magnitude of the effect is different because the relative humidity in the ascent region is different to that of the background state. Specifically, the model predicts that the midtropospheric relative humidity in the ascent region is higher than in the background state (Fig. 5), implying that the ascent

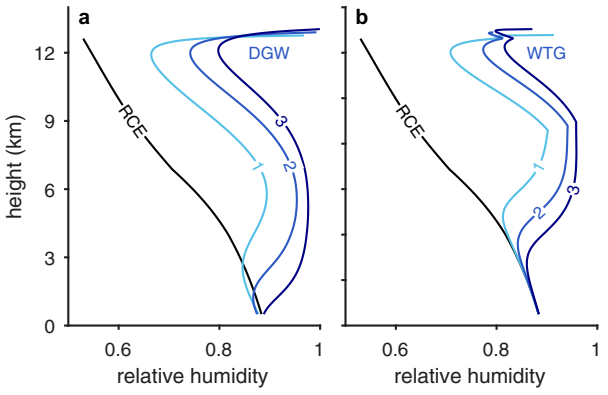

FIG. 5. Profiles of relative humidity according to the CZBP model under the (a) DGW and (b) WTG parameterizations (blue lines) with temperature anomalies at 8 km of $\Delta T_{\mathrm{ref}} = 1$, 2, and 3 K as labeled. The black line shows RCE solution.

region has a smaller (more stable) lapse rate, and providing an explanation for the strong increase with height of $\Delta T(z)$. Furthermore, the changes in relative humidity of the ascent region with ΔT_{ref} are nonlinear; in the lower troposphere, $\mathcal{R}(z)$ remains similar to its RCE value when ΔT_{ref} is small, and it only begins to increase when the magnitude of $\Delta T_{\mathrm{ref}} \gtrsim 2$ K. This nonlinearity helps to explain the changes in the shape of the profile of $\Delta T(z)$ discussed above.

We next consider the profiles of the large-scale vertical velocity $w(z)$. Both the WTG and DGW solutions show ascent over most of the troposphere, with vertical velocity profiles that are "top heavy," peaking at roughly 9 km (Fig. 6). For the WTG parameterization, the vertical velocity at a given level z is proportional to the temperature anomaly $\Delta T(z)$. The profile of $w(z)$, with small values in the lower troposphere and a sharp peak in the upper troposphere, may therefore be understood to be a direct consequence of the profile of $\Delta T(z)$ modulated by an expression involving the lapse rate and time scale $\tau_{\mathrm{WTG}}(z)$ in the denominator of (17). In the DGW case, the vertical velocity is related to $\Delta T(z)$ through second-order differential equation, such that the temperature anomaly at one level affects the vertical velocity at multiple levels. This results in a smoother profile of $w(z)$.

By comparing the above results to the solutions for $\epsilon = 0$, we may deduce the role of entrainment in determining the large-scale vertical velocity profile according to the CZBP model. As noted previously, the $\epsilon = 0$ solutions are nearly linear in the magnitude of the temperature anomaly ΔT_{ref}, and we plot them as single curves on Figs. 6b and 6d. Furthermore, the CZBP model under zero entrainment has a close connection to the QE dynamics framework introduced by Neelin and Zeng (2000) and used in many theoretical studies of tropical dynamics (e.g., Zeng et al. 2000; Emanuel 2007; Levine and Boos 2016;Wills et al. 2017). Like the $\epsilon = 0$ solutions, QE dynamics requires that the tropospheric lapse rate always remains close to that of a moist adiabat. This leads to a truncated set of equations for describing tropical overturning circulations in which the vertical velocity is represented by a single first-baroclinic-mode structure function. As shown in

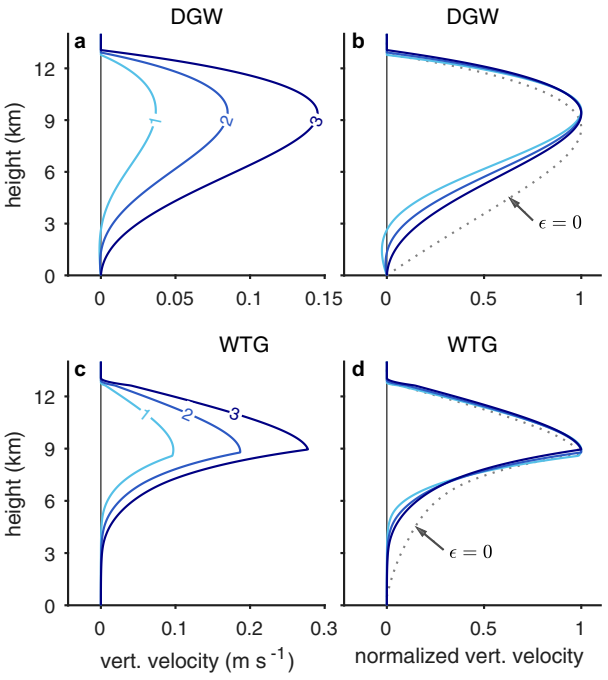

FIG. 6. As in Fig. 4, but for profiles of (a),(c) vertical velocity and (b),(d) vertical velocity normalized by its maximum value.

appendix C, this structure function is identical to the $\epsilon = 0$ solution for $w(z)$ under the DGW parameterization. The CZBP model under the DGW parameterization may therefore be seen as an extension of the QE dynamics framework to include the effects of convective entrainment.

In both the WTG and DGW cases, entrainment leads to a more top-heavy profile of $w(z)$. Although this only marginally affects the level at which $w(z)$ maximizes, it has a strong effect on the size of the vertical velocity within the lower troposphere relative to that in the upper troposphere. For example, negative (downward) vertical velocities appear at low levels in the DGW solutions for $\Delta T_{\mathrm{ref}} \leq 2$ K, extending up to 3 km for the case with $\Delta T_{\mathrm{ref}} = 1$ K. On the other hand, when ϵ is set to zero, the vertical velocity is positive at all levels. These results are not sensitive to the profile of entrainment assumed in the CZBP model. Alternate calculations in which the entrainment rate was assumed to vary according to $\epsilon \propto 1/z$ showed vertical velocity profiles with a similar increase in top-heaviness relative to the no entrainment case (not shown).

The top-heaviness of the vertical velocity profile is of particular importance for determining the energy transport associated with large-scale overturning circulations in the tropics because it affects the gross moist stability (Neelin and Held 1987; Raymond et al. 2009). According to the CZBP model, moist convective entrainment plays an important role in controlling the $w(z)$ profile, and therefore in controlling the gross moist stability. Note, however, that entrainment does not play a major role in explaining the differences in the vertical velocity profiles obtained using the DGW and WTG methods. Both with and without entrainment, the WTG solution has a much more top-heavy structure and a sharper peak of $w(z)$ in

the upper troposphere than the corresponding DGW solution. These differences are largely a result of the differences between the dynamical models (15) and (19) irrespective of the details of the thermodynamic model. Comparing to estimates of observed profiles of large-scale ascent (Handlos and Back 2014), it is the DGW profiles that appear more realistic.

Combining the results above, we may summarize the response of the CZBP model to an imposed midtropospheric temperature anomaly ΔT_{ref} as follows:

1) The imposed anomaly ΔT_{ref} implies that the atmosphere is warmer than the tropical mean in the midtroposphere. According to the dynamic model, this results in large-scale upward motion.
2) Under large-scale ascent, moistening of the environment through convective detrainment increases relative to drying of the environment by subsidence, and the thermodynamic model predicts that the relative humidity of the ascent region is higher than the tropical mean (Singh et al. 2019).
3) According to the ZBP approximation, a higher relative humidity is associated with a stabilization of the atmosphere. This results in the ascending region having a smaller lapse rate than that of the tropical mean, leading to the temperature anomaly $\Delta T(z)$ being large at upper levels relative to lower levels.
4) According to the dynamic model, a temperature anomaly profile that is upper-troposphere amplified leads to a top-heavy vertical velocity profile, with weak, or even downward vertical motion at low levels and strong ascent aloft.

While we have shown results based on temperature anomalies ΔT_{ref} imposed at $z_{\text{ref}} = 8$ km, the CZBP model may be solved for a variety of different reference levels. In general, the model produces top-heavy vertical velocity profiles with maxima near 9 km irrespective of whether the reference level is in the upper or lower troposphere. But there are also some important sensitivities to z_{ref}. For example, for a given value of ΔT_{ref}, taking $z_{\text{ref}} = 3$ km results in stronger ascent than for the $z_{\text{ref}} = 8$ km case, while the negative vertical velocities at low levels discussed above are eliminated from the solution. This is because, in the $z_{\text{ref}} = 3$ km case, the temperature anomaly $\Delta T(z)$ at 3 km is by definition positive, while it is close to zero or negative in the $z_{\text{ref}} = 8$ km solutions. Since ascending motion in the CZBP model solutions is associated with positive temperature anomalies in the middle to upper troposphere but may be associated with either positive or negative temperature anomalies in the lower troposphere, we focus on the $z_{\text{ref}} = 8$ km solutions here and in our comparison to CRM simulations below.

A key aspect of the CZBP model is that it provides a framework to understand the effects of convective mixing and microphysical processes, as represented by the entrainment rate ϵ and evaporation parameter μ, on the large-scale thermodynamic and dynamic structure of the tropical atmosphere. In the next section, we demonstrate the utility of this framework by comparing the predictions of the CZBP model to those based on simulations using a CRM with a parameterized large-scale circulation. Before we do so, however, we briefly evaluate the self-consistency of the model with respect to the assumption that $\epsilon = \delta$.

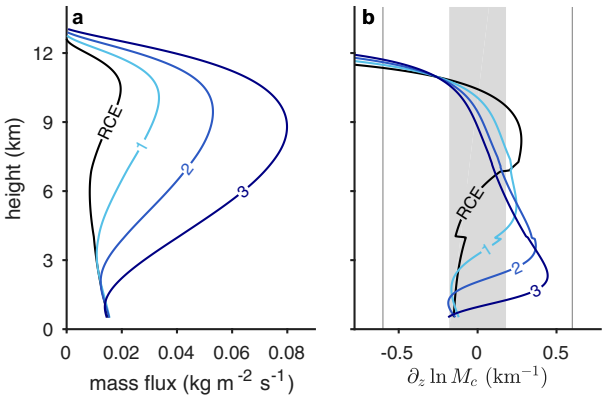

FIG. 7. (a) Convective mass flux $M_c(z)$ and (b) fractional vertical derivative of the convective mass flux $\partial_z \ln M_c$ according to the CZBP model for the RCE case (black) and for the DGW parameterization (blue) with temperature anomalies at 8 km of 1, 2, and 3 K as labeled. Gray lines in (b) mark the location where $|\partial_z \ln M_c| = \epsilon$ and gray shading shows regions where $|\partial_z \ln M_c| < 0.3\epsilon$.

c. *Self-consistency*

In solving the thermodynamic model, the fractional entrainment and detrainment rates were assumed to be equal, and the fractional vertical gradient of the convective mass flux $\partial_z \ln M_c$ was neglected in (12). To evaluate the validity of this assumption, we use (A13) to calculate the vertical profile of the convective mass flux for the solutions described in the previous subsection (Fig. 7a). We focus on the RCE solution and the solution calculated under the DGW parameterization because the associated vertical velocity profiles are more representative of observational estimates of large-scale ascent (see, e.g., Handlos and Back 2014) than for the WTG case. For the RCE state, $M_c(z)$ varies relatively weakly through most of the troposphere, except near the tropopause where the mass flux decreases to zero. In the DGW solutions, the domain experiences net ascent, and the mass flux is increased relative to RCE, particularly in the middle and upper troposphere. While the precise shape of the mass-flux profile is dependent on the entrainment formulation we use, we find similar mass-flux profiles when the entrainment is assumed to be proportional to $1/z$ rather than constant with height (not shown).

The mass-flux profiles associated with large-scale ascent in Fig. 7a differ somewhat from recent observational estimates of mass fluxes in convecting regions in the tropics, which generally show a rapid increase from the surface to the lower troposphere (3–4 km) and a gradual decrease above (Kumar et al. 2015; Schiro et al. 2018; Savazzi et al. 2021). This discrepancy may partially be a result of different definitions of mass flux; observational studies generally use a cloud updraft–based definition, which may not capture all of the ascending air, while in our case $M_c(z)$ represents the

ascending part of the domain and must be larger in magnitude than the net mass flux given by ρw. However, the discrepancy may also indicate differences between observed ascent profiles and those given by the CZBP model; detailed comparison of the CZBP model to observations is left for future work.

The mass-flux profiles demonstrate that the approximation $\epsilon = \delta$ is relatively well justified for the RCE case and for the DGW case with the weakest imposed temperature anomaly. In these cases, $|\partial_z \ln M_c| \lesssim 0.3\epsilon$ over most of the troposphere (Fig. 7b), allowing this term to be neglected in (12). The exception is near the tropopause; as already discussed, $M_c \to 0$ at the tropopause, and the fractional detrainment rate required to satisfy (12) becomes large, implying a failure of the assumption $\epsilon = \delta$, and rendering the solution for relative humidity inaccurate. At these levels, however, the smallness of the saturation humidity implies that variations in relative humidity have a negligible effect on the lapse rate, and this inaccuracy is unlikely to strongly affect the temperature anomaly profile $\Delta T(z)$ or the resultant vertical velocity profile.

For cases with stronger imposed temperature anomalies, the fractional variation of the convective mass flux becomes significant, with values of $\partial_z \ln M_c$ approaching the fractional entrainment rate in the lower troposphere. Specifically, the magnitude of $\partial_z \ln M_c$ reaches maximum values of 0.6ϵ and 0.7ϵ for $\Delta T_{\text{ref}} = 2$ and 3 K, respectively. In these cases, assuming $\epsilon = \delta$ introduces some error into the solution. Keeping in mind the potential influence of such errors, we now compare the CZBP solution to simulations using a CRM.

4. Comparison to cloud-permitting simulations

a. Model description

We perform simulations of a region of the atmosphere experiencing large-scale ascent using a CRM coupled to the DGW and WTG parameterizations. The model used is version 6.11.3 of the System for Atmospheric Modeling (SAM; Khairoutdinov and Randall 2003). SAM solves equations for the momentum, liquid/ice water static energy, water vapor, and precipitating and nonprecipitating condensate in three dimensions under the anelastic approximation. Shortwave and longwave radiative transfer is parameterized using the Rapid Radiative Transfer Model (RRTM; Clough et al. 2005), and cloud microphysics is treated using a one-moment scheme in which the hydrometeor partitioning is defined as a simple function of temperature. The effect of subgrid-scale motions is accounted for via a Smagorinsky turbulence scheme, but there is no explicit boundary layer parameterization.

We conduct simulations on a doubly periodic square domain with 96 grid points in each horizontal direction and 74 vertical levels. The horizontal grid spacing is 1 km and the vertical grid spacing increases from 75 m at the surface to 500 m at 3 km, remaining constant to the model top of 33 km. The lower boundary is a water surface held at a fixed temperature. Turbulent fluxes of momentum, energy, and water vapor between the surface and the atmosphere are evaluated using bulk aerodynamic formulas with exchange coefficients estimated using Monin–Obukhov similarity theory. For the calculation of the surface fluxes, a minimum wind speed of 1 m s^{-1} is assumed. Newtonian damping is applied to the upper 30% of the domain to minimize gravity wave reflection from the rigid-lid upper boundary. We neglect the effects of Earth's rotation by setting the Coriolis parameter to zero. The model configuration used here is identical to that of Singh et al. (2019), but rather than simulating the convective response to an imposed vertical velocity profile, we couple the model to large-scale dynamics using the DGW and WTG parameterizations.

b. Simulation design

To apply the DGW and WTG parameterizations, we first calculate a background state, representing the tropical mean, by simulating a state of RCE. For the RCE simulation, the surface temperature is set to 300 K, and following the RCEMIP protocol (Wing et al. 2018), the model is initialized with analytic profiles of temperature and humidity and seeded with random noise in the temperature field to initiate convection. The model is then run for 100 days with no diurnal cycle; solar insolation is assumed to be fixed to 551.58 W m^{-2} at a zenith angle of 42.05°. The horizontal and time mean from the last 50 days of this RCE simulation is taken to be the background state.

Simulations of the ascent region are then conducted by increasing the surface temperature by 1 K, reinitializing the model from the background state, and applying either the DGW or WTG parameterization. In both cases, a large-scale vertical velocity profile $w(z)$ is calculated at each model time step based on the mean thermodynamic profile of the model and that of the background state. This vertical velocity is then used to calculate advective tendencies of liquid/ice water static energy adv_h and specific humidity adv_q,

$$\text{adv}_h = -w(z)\left(\Gamma_d + \frac{\partial T}{\partial z}\right),$$

$$\text{adv}_q = -w(z)\frac{\partial q}{\partial z},$$

which are added to the relevant prognostic equations within the model. Here T and q are the horizontal-mean temperature and specific humidity in the simulation, respectively. This implementation neglects advection of condensed water species by the large-scale vertical velocity, and it neglects horizontal variations in temperature and specific humidity when calculating the advective tendencies.

In the WTG case, the vertical velocity $w(z)$ is calculated using (17), with T given by the horizontal-mean temperature of the simulation and T_0 given by the temperature of the reference state. We set the height to which (17) is applied to z_t = 14 km, given by the level at which the lapse rate in the background state decreases to 2 K km^{-1}. In the DGW case, the vertical velocity $w(z)$ is calculated using an equation similar to (19), but the temperatures T and T_0 are replaced by their corresponding virtual temperatures to account for the effect of water vapor on density, and we set z_t = 20 km. All other

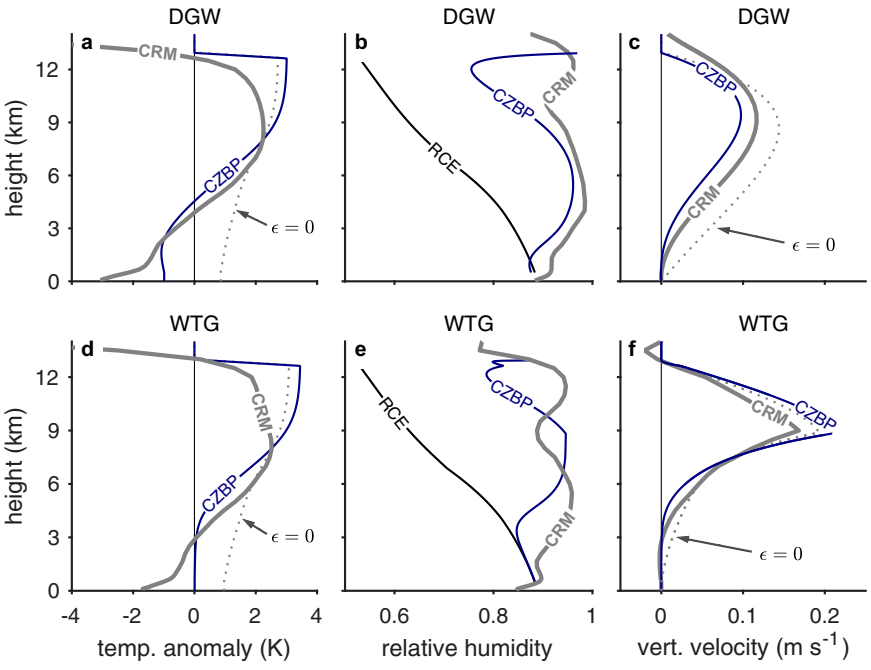

FIG. 8. Profiles of (a),(d) temperature anomaly $\Delta T(z)$, (b),(e) relative humidity $\mathcal{R}(z)$, and (c),(f) vertical velocity $w(z)$ under the (top) DGW and (bottom) WTG methods according to the CZBP model (blue) and in CRM simulations (gray). Simulated profiles are taken as the horizontal and time mean over days 50–100 and the CZBP model is solved with the temperature anomaly at 8 km equal to that of the corresponding CRM simulation. Note that (b) and (e) show the relative humidity of the RCE background state $\mathcal{R}_0(z)$ according to the CZBP model in black. Dotted lines in (a), (c), (d), and (f) show CZBP model solution with the entrainment rate $\varepsilon = 0$.

parameters for both the DGW and WTG parameterizations are identical to those in Table 1.

The WTG and DGW simulations represent estimates of the response of the atmosphere to a localized 1-K increase in the SST, and on physical grounds we expect the large-scale vertical velocity to be characterized by ascent through most of the troposphere. We run each case for 100 days, and we take the mean over the last 50 days to represent the steady-state response, which we will compare to the solution of the CZBP model below.

c. *Comparison of CZBP and cloud-permitting simulations*

We first compare the CZBP model to the CRM for the RCE background state. The mean temperature and relative humidity profiles of the RCE simulation are well reproduced by the CZBP model (Fig. 3). To some extent, this is to be expected since the radiation parameters of the CZBP model were set to roughly match the mean radiative cooling profile in the RCE simulation (Fig. 1) and the parameters ϵ and μ were optimized to reproduce the simulated RCE state as described in appendix B. But even taking these parameter choices into account, the ability of the CZBP model to reproduce the vertical structure of the background state relative humidity $\mathcal{R}_0(z)$ is impressive given its simplicity.

Since the entrainment and evaporation parameters were fixed based on the RCE background state, a more challenging test of the CZBP model is to examine the WTG and DGW cases. Figure 8 shows the mean profiles of the temperature anomaly $\Delta T(z)$, relative humidity $\mathcal{R}(z)$, and large-scale vertical velocity $w(z)$ in the CRM simulations and according to the CZBP model for both dynamic models. Here, the CZBP model is solved by setting ΔT_{ref}, the value of the temperature perturbation at the reference height $z_{\text{ref}} = 8$ km, to match the corresponding temperature perturbation in the simulations. Specifically, we set ΔT_{ref} equal to 2.23 and 2.52 K in the DGW and WTG cases, respectively.

The CZBP model reproduces a number of important features of the simulated thermodynamic profiles (Figs. 8a,b,d,e). For both the CRM and CZBP model, the temperature anomaly profile $\Delta T(z)$ is amplified in the upper troposphere, and the tropospheric relative humidity is higher in the ascending region than in the RCE background state. For the CRM simulations, the temperature anomaly profile is negative at low levels for both the DGW and WTG cases, and this is reproduced by the CZBP model for the DGW case. Under both dynamical models, the CZBP solution with entrainment provides a better reproduction of the CRM results than the $\epsilon = 0$ case. This provides evidence for a role of entrainment in setting the lapse rate of the ascending region of large-scale circulations, even when the effects of gravity waves in redistributing buoyancy anomalies is taken into account.

The CZBP model is also able to reproduce important characteristics of the simulated vertical velocity profiles (Figs. 8c,f), including the main differences between the DGW and WTG cases, and the increased top-heaviness of the profiles relative to the $\epsilon = 0$ solution. For the DGW method, the vertical velocity profile given by the $\epsilon = 0$ solution corresponds to the first-baroclinic mode structure of QE dynamics (see appendix C). The fact that both the CZBP model and CRM give $w(z)$ profiles that are more top-heavy than the QE first-baroclinic mode indicates the importance of considering convective entrainment in determining the vertical structure of the large-scale overturning circulation. Indeed, given the importance of the vertical structure of $w(z)$ for the gross moist stability, our results also point to a role for entrainment in determining energy transport within and out of the tropics.

The region where the results of the CZBP model and CRM are most different is in the upper troposphere ($z \gtrsim 9$ km), where the CZBP model overestimates the temperature anomaly $\Delta T(z)$. Previous studies have noted that the coupling between convection and the lapse rate is weaker in the upper troposphere compared to the lower troposphere (Kuang 2008b; Tulich and Mapes 2010), allowing other effects, such as radiation, to play a role in determining the temperature anomaly. Since the CZBP model does not include such effects, it is unsurprising that it is less accurate in the upper troposphere.

For the DGW case, the CZBP model underestimates the magnitude of the simulated vertical velocity as well as the height to which positive values of $w(z)$ extend. This is partially related to the differences in the $\Delta T(z)$ profiles described above, but it is also because, in the CZBP model, we apply the upper boundary condition on (19) at the tropopause, above which $\Delta T(z) = 0$. In the simulations, (19) is solved for heights between the surface and 20 km, and the vertical velocity is also influenced by temperature anomalies that exist above the tropopause.

Given the approximations inherent in the CZBP model, in particular, the crudeness of its representation of condensate re-evaporation, the neglect of the vertical variation of the convective mass flux, and the overall simplicity of the steady-state bulk-plume approach, the model provides a remarkable reproduction of the thermodynamic and dynamic profiles simulated by the CRM. This suggests that the CZBP model may be useful for understanding observed tropical circulations. A key challenge to such applications is that the WTG and DGW methods represent severely truncated representations of the dynamics; applying the CZBP framework developed here to more complete dynamical treatments is therefore an important avenue for future work.

5. Summary and discussion

We have constructed a simple steady-state model for the interaction between moist convection and large-scale ascent in the tropics. The model applies the ZBP approximation to determine the temperature and humidity profiles in a region of ascent, and it applies the WTG and DGW parameterizations to couple these thermodynamic profiles to the large-scale circulation. The CZBP model thereby provides a framework for relating the effects of mixing and microphysics in moist convection to the large-scale thermodynamic and dynamic structure of the atmosphere.

According to the CZBP model, convective entrainment and detrainment, respectively, result in a stabilization and moistening of the ascent region of a large-scale circulation relative to the tropical-mean background state. The stabilization affects the shape of the vertical velocity profile, causing it to become increasingly top-heavy. In particular, under the DGW parameterization, the vertical velocity is found to correspond to the first-baroclinic-mode structure of QE dynamics when the entrainment rate is set to zero and the tropospheric lapse rates of both the ascent region and the tropical mean state are assumed to be moist adiabatic. When entrainment is included, the vertical velocity in the lower troposphere is reduced relative to that in the upper troposphere, and if the circulation is not too strong, the vertical velocity even becomes negative at low levels.

The results of the CZBP model were found to be consistent with the behavior of CRM simulations in which the large-scale circulation is parameterized, building confidence in the applicability of the CZBP model to problems of relevance for the tropical atmosphere. In particular, the model may provide a link between the details of convective-scale mixing and the gross moist stability of the resultant convectively coupled large-scale circulation. The gross moist stability is of particular importance for understanding energy transport within the tropics (e.g., Neelin and Held 1987; Raymond et al. 2009) and in theories of intraseasonal variability (e.g., Raymond and Fuchs 2009).

Kuang (2011) also developed a theory for the gross moist stability based on the DGW representation of tropical dynamics. He showed that the top-heaviness of the vertical velocity profile increased with the wavenumber k and attributed this to the larger temperature anomalies required to maintain a given divergent flow at longer wavelengths. In the CZBP model, the magnitude of the temperature anomalies are set by the imposed value of ΔT_{ref}. Nevertheless, preliminary investigations indicate that, consistent with Kuang (2011), the top-heaviness of the vertical velocity $w(z)$ is reduced for smaller values of k at a fixed entrainment rate, and the profile approaches the QE first-baroclinic-mode profile given by the $\epsilon = 0$ solution as $k \to 0$. A detailed investigation of this wavelength dependence is beyond the scope of the current manuscript.

Our results provide support for the application of the ZBP approximation in determining the lapse rate locally within convecting regions of the tropics. Romps (2021) recently questioned such an application, arguing that the required horizontal gradients in temperature are larger than those observed. For the cases we considered, both the CZBP model and CRM simulations imply horizontal temperature differences of 2–4 K in the upper troposphere; Bao and Stevens (2021) found that temperature and virtual temperature anomalies of this magnitude were present along the equator in a global cloud-permitting simulation, but only on planetary scales. Consistent with this, Ahmed et al. (2021) used a linear

equatorial beta-plane model to argue that local convective adjustment of the tropospheric lapse rate is a good approximation for disturbances with sufficiently long wavelengths. Determining the precise spatial scales over which the ZBP approximation may be relevant in the tropics requires careful observational investigation that we hope to pursue in future work. Promisingly, a number of previous studies have reported negative correlations between lower-tropospheric stability and humidity in convective regions that are at least qualitatively consistent with the CZBP model (Singh and O'Gorman 2013; Gjorgjievska and Raymond 2014; Raymond et al. 2015; Raymond and Fuchs-Stone 2021).

A surprising aspect of the CZBP solutions is that they suggest that the ascent region has a similar or lower temperature than the tropical mean at low levels, and for the DGW parameterization, this leads to downward vertical motion at these levels. While similar low-level cold anomalies coupled with descent were also found in the CRM simulations (see also Kuang 2011), observed tropical ascent regions occur where the boundary layer is anomalously warm and moist (Nie et al. 2010) and are characterized by upward motion at all levels within the troposphere (Handlos and Back 2014). Preliminary analysis indicates that low-level descent is not present for the DGW parameterization when the wavenumber k is decreased (see also Kuang 2011), and this further suggests that the CZBP model may be most applicable to planetary-scale flows.

The CZBP solutions are governed by the external parameter ΔT_{ref}, which here we take as the temperature anomaly in the middle troposphere. Ideally, one would connect the dynamic and thermodynamic structure of the atmosphere directly to imposed SST anomalies for a closer analog to the CRM simulations. But developing such a connection is made difficult by the opposite signed temperature anomalies in the upper and lower troposphere already mentioned. A theoretical model that directly connects the dynamic response of the atmosphere to imposed SST anomalies remains the subject of ongoing work.

A limitation of the CZBP model is that the WTG and DGW dynamic models that allow for coupling to the large-scale circulation represent truncations of the full dynamical equations; real overturning circulations include a range of wavenumbers and cannot be represented by a relaxation to the tropical-mean profile over a single time scale. Moreover, our framework neglects the role played by balanced dynamics in influencing the atmospheric thermal structure highlighted recently by Raymond et al. (2015), but its reliance on the steady-state assumption renders it applicable only to circulations that evolve sufficiently slowly (Singh et al. 2019). Finally, the CZBP model does not account for known differences in the efficiency with which convection couples to the large-scale thermodynamic state in the lower troposphere compared to the upper troposphere (e.g., Kuang 2008b; Tulich and Mapes 2010). These limitations may prevent the CZBP model from admitting solutions comprising "shallow" circulations, in which the vertical velocity profile peaks in the lower troposphere, that are known to be important for understanding the tropical precipitation distribution (Back and Bretherton 2009b,a; Duffy et al. 2020).

Despite the above caveats, future work to apply the CZBP model to a wider range of circumstances represents a promising avenue for understanding the interaction between moist convection and large-scale circulations in the tropics. In particular, a forthcoming manuscript by the authors (Neogi and Singh 2022) applies the ZBP approximation to help understand how the large-scale tropical circulation responds to local versus global changes in surface temperature.

Acknowledgments. The authors acknowledge support from the Australian Research Council (Grants DE190100866, DP200102954, and CE170100023) and computational resources and services from the National Computational Infrastructure (NCI), both supported by the Australian government. The authors thank Ji Ne and two anonymous reviewers for comments that helped improve the manuscript.

Data availability statement. Simulation data and codes used in this work are available from the Monash Bridges repository at https://doi.org/10.26180/19428704.v1.

APPENDIX A

Solution of the Thermodynamic Model

Here we provide details of the solution of the thermodynamic model. We first solve for the relative humidity and lapse rate at a given level. We then show how this solution may be integrated vertically to provide profiles of temperature and relative humidity for a given vertical velocity profile.

a. Solution at a given level

Following Romps (2021), we derive an equation for the relative humidity in terms of only T, p, ϵ, δ, μ, the radiative cooling rate Q_{rad}, and vertical velocity w. The expression for the relative humidity (7) contains the unknowns γ and r. Combining (8) and (10), we may write

$$\gamma = \gamma_m + \epsilon b(1 - \mathcal{R}), \tag{A1}$$

where

$$\gamma_m = \frac{L_v}{R_v T^2}\left(\Gamma_m - \frac{g}{R_d T}\right)$$

is the fractional saturation specific humidity gradient along a moist adiabat, and

$$b(T,p) = \frac{L_v^2 q^*}{c_p R_v T^2 + L_v^2 q^*}$$

is a nondimensional thermodynamic function. Substituting (A1) into the expression for the relative humidity (7), we may write

$$\mathcal{R} = \frac{\delta(1+\mu)}{\delta(1+\mu) + r[\gamma_m + \epsilon b(1-\mathcal{R})]}. \tag{A2}$$

The remaining task is to express r in terms of known quantities. To do so, we combine (6a) and (5) to write down an equation for the net condensation rate $s_{\text{net}} = s_{\text{cond}} - s_{\text{evap}}$:

$$s_{\text{net}} = [\gamma - (\epsilon + \mu\delta)(1 - \mathcal{R})]M_c q^*. \tag{A3}$$

Using (1), we have $\rho w = (1 - r)M_c$, and therefore

$$s_{\text{net}} = \frac{1}{1 - r}\left[\gamma - (\epsilon + \mu\delta)(1 - \mathcal{R})\right]\rho w q^*. \tag{A4}$$

We now use (6a)–(6d) to derive a second expression for s_{net}. Subtracting L_v times (6a) from (6c) and L_v times (6b) from (6d) gives equations for the dry static energy budgets of the convective region and environment:

$$M_c \frac{\partial s}{\partial z} = L_v s_{\text{cond}}, \tag{A5}$$

$$M_e \frac{\partial s}{\partial z} = -L_v s_{\text{evap}} + Q_{\text{rad}}, \tag{A6}$$

where $s = c_p T + gz$ is the dry static energy. Multiplying (A5) by $r = -M_e/M_c$ and adding it to (A6) we have, with some rearrangement,

$$s_{\text{net}} = -\frac{1}{r}\left[\frac{Q_{\text{rad}}}{L_v} - \mu\delta\rho w(1 - \mathcal{R})q^*\right]. \tag{A7}$$

Combining the expressions (A4) and (A7) for the net condensation rate and using (A1), we may write

$$\frac{\gamma_m - (\epsilon - \epsilon b + \mu\delta)(1 - \mathcal{R})}{\dfrac{Q_{\text{rad}}}{L_v \rho w q^*} - \mu\delta(1 - \mathcal{R})} = -\frac{1 - r}{r}. \tag{A8}$$

The final step is to combine the above equation with (A2). To do so, we solve (A2) for r:

$$r = \frac{\delta(1 + \mu)(1 - \mathcal{R})}{\mathcal{R}\left[\gamma_m + \epsilon b(1 - \mathcal{R})\right]}. \tag{A9}$$

Subtracting (A9) from one and dividing by (A9) gives

$$\frac{-\epsilon b\mathcal{R}^2 + \left[\gamma_m + \epsilon b + \delta(1 + \mu)\right]\mathcal{R} - \delta(1 + \mu)}{\delta(1 + \mu)(1 - \mathcal{R})} = \frac{1 - r}{r}. \tag{A10}$$

We may then equate the left-hand side of (A8) with the negative of the left-hand side of (A10) to give a cubic for the relative humidity $\mathcal{R}$,

$$a_3\mathcal{R}^3 + a_2\mathcal{R}^2 + a_1\mathcal{R} + a_0 = 0, \tag{A11}$$

where

$$a_3 = \hat{\epsilon} b\left(\frac{\mu}{1 + \mu}\right)\hat{w},$$

$$a_2 = \frac{\hat{\epsilon} b}{\hat{\delta}(1 + \mu)} + \left[\hat{\epsilon}(1 - b) - (1 + 2\hat{\epsilon} b)\left(\frac{\mu}{1 + \mu}\right)\right]\hat{w},$$

$$a_1 = -\left[1 + \frac{1 + \hat{\epsilon} b}{\hat{\delta}(1 + \mu)}\right] + \left[\hat{\epsilon}(b - 2) + (1 + \hat{\epsilon} b)\left(\frac{1 + 2\mu}{1 + \mu}\right)\right]\hat{w},$$

$$a_0 = 1 + \left[\hat{\epsilon}(1 - b) - 1\right]\hat{w}.$$

Here we have nondimensionalized the equation by defining $\hat{\epsilon} = \epsilon/\gamma_m$, $\hat{\delta} = \delta/\gamma_m$, and

$$\hat{w} = \frac{L_v q^* \gamma_m}{Q_{\text{rad}}}\rho w. \tag{A12}$$

Noting that the density may be expressed using the ideal gas law as $\rho = R_d T/p$, the coefficients a_i depend only on T, p, ϵ, δ, μ, Q_{rad}, and w. Given these quantities, (A11) may be solved using the cubic formula, and the lapse rate calculated via (10). Note also that (A1), (A3), and (A7) may be combined to give the convective mass flux:

$$M_c = -\frac{1}{r}\left[\frac{\dfrac{Q_{\text{rad}}}{L_v q^*} - \mu\delta\rho w(1 - \mathcal{R})}{\gamma_m - (\epsilon - \epsilon b + \mu\delta)(1 - \mathcal{R})}\right]. \tag{A13}$$

Once the relative humidity has been found using the procedure above, this equation may be solved for a given temperature and pressure using (A9) to evaluate r.

b. Integration in the vertical

To calculate the full thermodynamic profiles, we begin with the temperature and pressure at a reference level $z_{\text{ref}} = 8$ km. We then integrate the coupled set of equations

$$\frac{\partial T}{\partial z} = -\Gamma\left[T, p; w(z), \epsilon, \mu\right] \quad \text{and}$$

$$\frac{\partial p}{\partial z} = -\frac{pg}{R_d T}$$

upward and downward using a fourth-order Runge–Kutta method with a step size of 20 m. The lapse rate Γ is calculated via (10), with the relative humidity evaluated by solving the cubic (A11), Q_{rad} evaluated based on (13), and taking $\epsilon = \delta$. The integration may then be performed for a given profile of vertical velocity $w(z)$ and given values of the entrainment rate ϵ and evaporation parameter μ.

The integration continues upward until the temperature $T = T_t$; above this level the temperature is assumed to be constant and the relative humidity is undefined. The integration continues downward to the surface, but at levels below $z = z_b$ we set the lapse rate to its dry adiabatic value $\Gamma = \Gamma_d$, and we leave the relative humidity undefined.

APPENDIX B

Choice of Parameters in the Thermodynamic Model

The parameters for the thermodynamic model are chosen based on the domain- and time-mean thermodynamic profiles of a CRM simulation of RCE described in section 4.

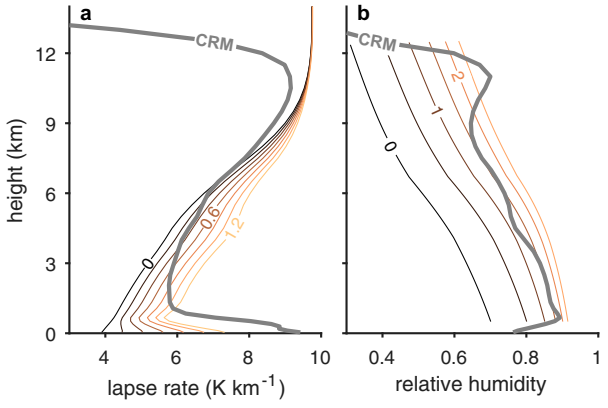

FIG. B1. Domain- and time-mean (a) temperature lapse rate and (b) relative humidity profiles in CRM simulation of RCE (gray). Colored lines show (a) the lapse rate according to (10) given the simulated profiles of temperature, pressure, and relative humidity and for entrainment rates varying from 0 to 1.2 km^{-1} as labeled, and (b) the relative humidity according to the thermodynamic model for $\epsilon = 0.6$ km^{-1} and evaporation parameter μ varying from 0 to 2.5 as labeled.

We first set $T_{\text{ref}} = 243.8$ K and $p_{\text{ref}} = 370$ hPa to match the temperature and pressure of the CRM simulation at the level $z_{\text{ref}} = 8$ km. Next, we set the entrainment rate ϵ by comparing the simulated lapse rate to that calculated from (10) using a range of entrainment rates and taking the simulated temperature, pressure, and relative humidity as inputs (Fig. B1a). At levels just above the boundary layer, the simulated lapse rate roughly matches that given by (10) for an entrainment rate of ~1.2 km^{-1}. But the diagnosed entrainment rate decreases with height, and above ~7 km the simulated lapse rate is smaller than the moist adiabatic lapse rate Γ_m and cannot be reproduced by (10) for any positive entrainment. Zhou and Xie (2019) show how this upper-tropospheric stability may be understood within the zero-buoyancy plume framework by considering multiple plumes with different entrainment rates, rather than a single bulk plume. According to their model, each plume detrains at a different height given by its level of neutral buoyancy, allowing the lapse rate to be smaller than in any individual plume. Here we retain the simpler bulk-plume approach, and we take a value of $\epsilon = 0.6$ km^{-1} based on the simulated lapse rate in the lower troposphere. As shown in Fig. 3, the resultant solution to the CZBP model provides a good match to the temperature structure of the RCE simulation over most of the troposphere.

Having set the entrainment rate, we now set the evaporation parameter μ. We solve the thermodynamic model with $\epsilon = 0.6$ km^{-1} and for a range of evaporation parameters μ for the case of RCE [$w(z) = 0$]. According to the thermodynamic model, the relative humidity $\mathcal{R}$ increases with increasing μ (Fig. B1b). We find that a value of $\mu = 1.5$ gives a good match between the relative humidity simulated by the CRM and that given by the thermodynamic model. The values of ϵ and μ chosen here are then used for all further calculations with the thermodynamic model.

APPENDIX C

Connection to Quasi-Equilibrium Dynamics

Here we show that the vertical velocity profiles produced by the CZBP model for zero entrainment and under the DGW parameterization have the same vertical structure as the first-baroclinic mode described by quasi-equilibrium (QE) dynamics (Neelin and Zeng 2000; Emanuel 2007). The QE dynamics framework is based on the assumption that convection constrains the tropospheric lapse rate to be very nearly equal to the moist-adiabatic lapse rate Γ_m. Linearizing about the tropical-mean temperature profile $T_0(z)$, this allows temperature variations in the atmosphere to be approximated by a single vertical structure function $A(z)$ so that

$$T'(\mathbf{x}, z, t) = A(z)T^*(\mathbf{x}, t), \tag{C1}$$

where $T'(\mathbf{x}, z, t)$ is the perturbation temperature, equal to $T(\mathbf{x}, z, t) - T_0(z)$, and the function T^* depends only on horizontal position $\mathbf{x}$ and time t.

The assumption of a moist adiabatic lapse rate $\Gamma = \Gamma_m$ corresponds to the solution of the thermodynamic model for zero entrainment. We may therefore write the vertical structure function

$$A(z) \approx \frac{\Delta T_{\epsilon=0}(z)}{\Delta T_{\text{ref}}}, \tag{C2}$$

where $\Delta T_{\epsilon=0}(z)$ is the temperature anomaly according to the thermodynamic model for $\epsilon = 0$ and ΔT_{ref} is its value at the reference level.

The vertical structure of temperature variations given by (C2) places a strong constraint on the vertical structure of the winds. To see this, consider the linearized, inviscid anelastic equations for horizontal momentum, hydrostatic balance, and continuity—respectively,

$$\frac{\partial(\rho_0 \mathbf{v})}{\partial t} = -\nabla p', \tag{C3}$$

$$\frac{1}{\rho_0}\frac{\partial p'}{\partial z} = -g\frac{T'}{T_0}, \tag{C4}$$

$$\nabla \cdot (\rho_0 \mathbf{v}) + \frac{\partial(\rho_0 w)}{\partial z} = 0. \tag{C5}$$

Here $\mathbf{v}$ is the horizontal velocity, $p'(\mathbf{x}, z, t)$ is the perturbation pressure, and the subscript 0 refers to the tropical-mean background state. Following Kuang (2008a), we have neglected the contribution of the pressure perturbation to the buoyancy, and we further neglect virtual effects. Differentiating (C3) with respect to z and substituting (C4), we have

$$\frac{\partial}{\partial t}\left[\frac{\partial(\rho_0 \mathbf{v})}{\partial z}\right] = \nabla\left(\frac{\rho_0 g T'}{T_0}\right).$$

Applying the QE assumption using (C1) and (C2), we have

$$\frac{\partial}{\partial t}\left[\frac{\partial(\rho_0 \mathbf{v})}{\partial z}\right] = \left[\frac{\rho_0 \Delta T_{\epsilon=0}}{T_0}\right]\frac{g\nabla T^*(\mathbf{x},t)}{\Delta T_{\text{ref}}}.$$

Only the term in square brackets on the right-hand side of the above equation depends on height z. This implies that the QE constraint of moist-adiabatic lapse rates limits the vertical structure of the horizontal winds to two modes: a barotropic mode independent of height, and a baroclinic mode $V(z)$ defined by

$$\frac{\partial(\rho_0 V)}{\partial z} = \frac{\rho_0 \Delta T_{\epsilon=0}}{T_0}.$$

By continuity (C5), the baroclinic mode has an associated vertical velocity structure $W(z)$ that satisfies

$$\frac{\partial^2(\rho_0 W)}{\partial z^2} = -\frac{\rho_0 \Delta T_{\epsilon=0}}{T_0}.$$

Replacing ρ_0 with ρ, the above equation may be seen to give the same vertical structure as the DGW parameterization (19) for the case in which $\epsilon = 0$. A similar derivation of this baroclinic mode in pressure coordinates may be found in Neelin and Zeng (2000).

REFERENCES

Ahmed, F., and J. D. Neelin, 2018: Reverse engineering the tropical precipitation–buoyancy relationship. *J. Atmos. Sci.*, **75**, 1587–1608, https://doi.org/10.1175/JAS-D-17-0333.1.

——, ——, and Á. F. Adames, 2021: Quasi-equilibrium and weak temperature gradient balances in an equatorial beta-plane model. *J. Atmos. Sci.*, **78**, 209–227, https://doi.org/10.1175/JAS-D-20-0184.1.

Arakawa, A., and W. H. Schubert, 1974: Interaction of a cumulus cloud ensemble with the large-scale environment, part I. *J. Atmos. Sci.*, **31**, 674–701, https://doi.org/10.1175/1520-0469(1974)031<0674:IOACCE>2.0.CO;2.

Back, L. E., and C. S. Bretherton, 2006: Geographic variability in the export of moist static energy and vertical motion profiles in the tropical Pacific. *Geophys Res. Lett.*, **33**, L17810, https://doi.org/10.1029/2006GL026672.

——, and ——, 2009a: On the relationship between SST gradients, boundary layer winds, and convergence over the tropical oceans. *J. Climate*, **22**, 4182–4196, https://doi.org/10.1175/2009JCLI2392.1.

——, and ——, 2009b: A simple model of climatological rainfall and vertical motion patterns over the tropical oceans. *J. Climate*, **22**, 6477–6497, https://doi.org/10.1175/2009JCLI2393.1.

Bao, J., and B. Stevens, 2021: The elements of the thermodynamic structure of the tropical atmosphere. *J. Meteor. Soc. Japan*, **99**, 1483–1499, https://doi.org/10.2151/jmsj.2021-072.

Bretherton, C. S., and S. Park, 2008: A new bulk shallow-cumulus model and implications for penetrative entrainment feedback on updraft buoyancy. *J. Atmos. Sci.*, **65**, 2174–2193, https://doi.org/10.1175/2007JAS2242.1.

——, M. E. Peters, and L. E. Back, 2004: Relationships between water vapor path and precipitation over the tropical oceans. *J. Climate*, **17**, 1517–1528, https://doi.org/10.1175/1520-0442(2004)017<1517:RBWVPA>2.0.CO;2.

Charney, J. G., 1963: A note on large-scale motions in the tropics. *J. Atmos. Sci.*, **20**, 607–609, https://doi.org/10.1175/1520-0469(1963)020<0607:ANOLSM>2.0.CO;2.

Chou, C., and J. D. Neelin, 2004: Mechanisms of global warming impacts on regional tropical precipitation. *J. Climate*, **17**, 2688–2701, https://doi.org/10.1175/1520-0442(2004)017<2688:MOGWIO>2.0.CO;2.

Clough, S. A., M. W. Shephard, E. J. Mlawer, J. S. Delamere, M. J. Iacono, K. Cady-Pereira, S. Boukabara, and P. D. Brown, 2005: Atmospheric radiative transfer modeling: A summary of the AER codes. *J. Quant. Spectrosc. Radiat. Transfer*, **91**, 233–244, https://doi.org/10.1016/j.jqsrt.2004.05.058.

Daleu, C. L., and Coauthors, 2015: Intercomparison of methods of coupling between convection and large-scale circulation: 1. Comparison over uniform surface conditions. *J. Adv. Model. Earth Syst.*, **7**, 1576–1601, https://doi.org/10.1002/2015MS000468.

——, and Coauthors, 2016: Intercomparison of methods of coupling between convection and large-scale circulation: 2. Comparison over nonuniform surface conditions. *J. Adv. Model. Earth Syst.*, **8**, 387–405, https://doi.org/10.1002/2015MS000570.

Davies, L., C. Jakob, P. May, V. V. Kumar, and S. Xie, 2013: Relationships between the large-scale atmosphere and the small-scale convective state for Darwin, Australia. *J. Geophys. Res. Atmos.*, **118**, 11 534–11 545, https://doi.org/10.1002/jgrd.50645.

Duffy, M. L., P. A. O'Gorman, and L. E. Back, 2020: Importance of Laplacian of low-level warming for the response of precipitation to climate change over tropical oceans. *J. Climate*, **33**, 4403–4417, https://doi.org/10.1175/JCLI-D-19-0365.1.

Emanuel, K., 2007: Quasi-equilibrium dynamics of the tropical atmosphere. *The Global Circulation of the Atmosphere*, T. Schneider, and A. H. Sobel, Eds., Princeton University Press, 186–218.

——, 2019: Inferences from simple models of slow, convectively coupled processes. *J. Atmos. Sci.*, **76**, 195–208, https://doi.org/10.1175/JAS-D-18-0090.1.

——, J. D. Neelin, and C. S. Bretherton, 1994: On large-scale circulations in convecting atmospheres. *Quart. J. Roy. Meteor. Soc.*, **120**, 1111–1143, https://doi.org/10.1002/qj.49712051902.

Gjorgjievska, S., and D. J. Raymond, 2014: Interaction between dynamics and thermodynamics during tropical cyclogenesis. *Atmos. Chem. Phys.*, **14**, 3065–3082, https://doi.org/10.5194/acp-14-3065-2014.

Handlos, Z. J., and L. E. Back, 2014: Estimating vertical motion profile shape within tropical weather states over the oceans. *J. Climate*, **27**, 7667–7686, https://doi.org/10.1175/JCLI-D-13-00602.1.

Hartmann, D. L., J. R. Holton, and Q. Fu, 2001: The heat balance of the tropical tropopause, cirrus, and stratospheric dehydration. *Geophys. Res. Lett.*, **28**, 1969–1972, https://doi.org/10.1029/2000GL012833.

Holloway, C. E., and J. D. Neelin, 2009: Moisture vertical structure, column water vapor, and tropical deep convection. *J. Atmos. Sci.*, **66**, 1665–1683, https://doi.org/10.1175/2008JAS2806.1.

Khairoutdinov, M. F., and D. A. Randall, 2003: Cloud resolving modeling of the ARM summer 1997 IOP: Model formulation, results, uncertainties, and sensitivities. *J. Atmos. Sci.*, **60**, 607–625, https://doi.org/10.1175/1520-0469(2003)060<0607:CRMOTA>2.0.CO;2.

Kuang, Z., 2008a: Modeling the interaction between cumulus convection and linear gravity waves using a limited-domain cloud system–resolving model. *J. Atmos. Sci.*, **65**, 576–591, https://doi.org/10.1175/2007JAS2399.1.

——, 2008b: A moisture-stratiform instability for convectively coupled waves. *J. Atmos. Sci.*, **65**, 834–854, https://doi.org/10.1175/2007JAS2444.1.

——, 2011: The wavelength dependence of the gross moist stability and the scale selection in the instability of column-integrated moist static energy. *J. Atmos. Sci.*, **68**, 61–74, https://doi.org/10.1175/2010JAS3591.1.

Kumar, V. V., C. Jakob, A. Protat, C. R. Williams, and P. T. May, 2015: Mass-flux characteristics of tropical cumulus clouds from wind profiler observations at Darwin, Australia. *J. Atmos. Sci.*, **72**, 1837–1855, https://doi.org/10.1175/JAS-D-14-0259.1.

Kuo, Y.-H., K. A. Schiro, and J. D. Neelin, 2018: Convective transition statistics over tropical oceans for climate model diagnostics: Observational baseline. *J. Atmos. Sci.*, **75**, 1553–1570, https://doi.org/10.1175/JAS-D-17-0287.1.

Levine, X. J., and W. R. Boos, 2016: A mechanism for the response of the zonally asymmetric subtropical hydrologic cycle to global warming. *J. Climate*, **29**, 7851–7867, https://doi.org/10.1175/JCLI-D-15-0826.1.

Neelin, J. D., 2007: Moist dynamics of tropical convection zones in monsoons, teleconnections, and global warming. *The Global Circulation of the Atmosphere*, T. Schneider, and A. H. Sobel, Eds., Princeton University Press, 267–301, Chapter 10.

——, and I. M. Held, 1987: Modeling tropical convergence based on the moist static energy budget. *Mon. Wea. Rev.*, **115**, 3–12, https://doi.org/10.1175/1520-0493(1987)115<0003:MTCBOT>2.0.CO;2.

——, and N. Zeng, 2000: A quasi-equilibrium tropical circulation model—Formulation. *J. Atmos. Sci.*, **57**, 1741–1766, https://doi.org/10.1175/1520-0469(2000)057<1741:AQETCM>2.0.CO;2.

Neogi, S., and M. S. Singh, 2022: Understanding changes in the tropical circulation under global warming using a cloud-resolving model and a conceptual model. *J. Climate*, 10.1175/JCLI-D-21-0854.1, in press.

Nie, J., W. R. Boos, and Z. Kuang, 2010: Observational evaluation of a convective quasi-equilibrium view of monsoons. *J. Climate*, **23**, 4416–4428, https://doi.org/10.1175/2010JCLI3505.1.

Raymond, D. J., and X. Zeng, 2005: Modelling tropical atmospheric convection in the context of the weak temperature gradient approximation. *Quart. J. Roy. Meteor. Soc.*, **131**, 1301–1320, https://doi.org/10.1256/qj.03.97.

——, and Ž. Fuchs, 2009: Moisture modes and the Madden–Julian oscillation. *J. Climate*, **22**, 3031–3046, https://doi.org/10.1175/2008JCLI2739.1.

——, and Ž. Fuchs-Stone, 2021: Emergent properties of convection in OTREC and PREDICT. *J. Geophys. Res. Atmos.*, **126**, e2020JD033585, https://doi.org/10.1029/2020JD033585.

——, S. L. Sessions, A. H. Sobel, and Ž. Fuchs, 2009: The mechanics of gross moist stability. *J. Adv. Model. Earth Syst.*, **1**, 9, https://doi.org/10.3894/JAMES.2009.1.9.

Raymond, D., Ž. Fuchs, S. Gjorgjievska, and S. Sessions, 2015: Balanced dynamics and convection in the tropical troposphere. *J. Adv. Model. Earth Syst.*, **7**, 1093–1116, https://doi.org/10.1002/2015MS000467.

Romps, D. M., 2012a: Numerical tests of the weak pressure gradient approximation. *J. Atmos. Sci.*, **69**, 2846–2856, https://doi.org/10.1175/JAS-D-11-0337.1.

——, 2012b: Weak pressure gradient approximation and its analytical solutions. *J. Atmos. Sci.*, **69**, 2835–2845, https://doi.org/10.1175/JAS-D-11-0336.1.

——, 2014: An analytical model for tropical relative humidity. *J. Climate*, **27**, 7432–7449, https://doi.org/10.1175/JCLI-D-14-00255.1.

——, 2021: Ascending columns, WTG, and convective aggregation. *J. Atmos. Sci.*, **78**, 497–508, https://doi.org/10.1175/JAS-D-20-0041.1.

Savazzi, A. C. M., C. Jakob, and A. P. Siebesma, 2021: Convective mass-flux from long term radar reflectivities over Darwin, Australia. *J. Geophys. Res. Atmos.*, **126**, e2021JD034910, https://doi.org/10.1029/2021JD034910.

Schiro, K. A., J. D. Neelin, D. K. Adams, and B. R. Lintner, 2016: Deep convection and column water vapor over tropical land versus tropical ocean: A comparison between the Amazon and the tropical western Pacific. *J. Atmos. Sci.*, **73**, 4043–4063, https://doi.org/10.1175/JAS-D-16-0119.1.

——, F. Ahmed, S. E. Giangrande, and J. D. Neelin, 2018: GoAmazon2014/5 campaign points to deep-inflow approach to deep convection across scales. *Proc. Natl. Acad. Sci. USA*, **115**, 4577–4582, https://doi.org/10.1073/pnas.1719842115.

Seeley, J. T., and D. M. Romps, 2015: Why does tropical convective available potential energy (CAPE) increase with warming? *Geophys. Res. Lett.*, **42**, 10 429–10 437, https://doi.org/10.1002/2015GL066199.

Sessions, S. L., S. Sugaya, D. J. Raymond, and A. H. Sobel, 2010: Multiple equilibria in a cloud-resolving model using the weak temperature gradient approximation. *J. Geophys. Res.*, **115**, D12110, https://doi.org/10.1029/2009JD013376.

Singh, M. S., and P. A. O'Gorman, 2013: Influence of entrainment on the thermal stratification in simulations of radiative-convective equilibrium. *Geophys. Res. Lett.*, **40**, 4398–4403, https://doi.org/10.1002/grl.50796.

——, and ——, 2015: Increases in moist-convective updraught velocities with warming in radiative-convective equilibrium. *Quart. J. Roy. Meteor. Soc.*, **141**, 2828–2838, https://doi.org/10.1002/qj.2567.

——, Z. Kuang, E. D. Maloney, W. M. Hannah, and B. O. Wolding, 2017: Increasing potential for intense tropical and subtropical thunderstorms under global warming. *Proc. Natl. Acad. Sci. USA*, **114**, 11 657–11 662, https://doi.org/10.1073/pnas.1707603114.

——, R. A. Warren, and C. Jakob, 2019: A steady-state model for the relationship between humidity, instability, and precipitation in the tropics. *J. Adv. Model. Earth Syst.*, **11**, 3973–3994, https://doi.org/10.1029/2019MS001686.

Sobel, A. H., and C. S. Bretherton, 2000: Modeling tropical precipitation in a single column. *J. Climate*, **13**, 4378–4392, https://doi.org/10.1175/1520-0442(2000)013<4378:MTPIAS>2.0.CO;2.

Tulich, S. N., and B. E. Mapes, 2010: Transient environmental sensitivities of explicitly simulated tropical convection. *J. Atmos. Sci.*, **67**, 923–940, https://doi.org/10.1175/2009JAS3277.1.

Wang, S., and A. H. Sobel, 2011: Response of convection to relative sea surface temperature: Cloud-resolving simulations in two and three dimensions. *J. Geophys. Res.*, **116**, D11119, https://doi.org/10.1029/2010JD015347.

——, ——, and Z. Kuang, 2013: Cloud-resolving simulation of TOGA-COARE using parameterized large-scale dynamics. *J. Geophys. Res. Atmos.*, **118**, 6290–6301, https://doi.org/10.1002/jgrd.50510.

Warren, R. A., M. S. Singh, and C. Jakob, 2020: Simulations of radiative-convective-dynamical equilibrium. *J. Adv. Model. Earth Syst.*, **12**, e2019MS001734, https://doi.org/10.1029/2019MS001734.

Wills, R. C., X. J. Levine, and T. Schneider, 2017: Local energetic constraints on Walker circulation strength. *J. Atmos. Sci.*, **74**, 1907–1922, https://doi.org/10.1175/JAS-D-16-0219.1.

Wing, A. A., K. A. Reed, M. Satoh, B. Stevens, S. Bony, and T. Ohno, 2018: Radiative-Convective Equilibrium Model

Intercomparison Project. *Geosci. Model Dev.*, **11**, 793–813, https://doi.org/10.5194/gmd-11-793-2018.

Yin, Z., P. Dai, and J. Nie, 2021: A two-plume convective model for precipitation extremes. *Adv. Atmos. Sci.*, **38**, 957–965, https://doi.org/10.1007/s00376-021-0404-8.

Yu, J.-Y., and J. D. Neelin, 1997: Analytic approximations for moist convectively adjusted regions. *J. Atmos. Sci.*, **54**, 1054–1063, https://doi.org/10.1175/1520-0469(1997)054<1054:AAFMCA>2.0.CO;2.

Zeng, N., J. D. Neelin, and C. Chou, 2000: A quasi-equilibrium tropical circulation model—Implementation and simulation. *J. Atmos. Sci.*, **57**, 1767–1796, https://doi.org/10.1175/1520-0469(2000)057<1767:AQETCM>2.0.CO;2.

Zhou, W., and S.-P. Xie, 2019: A conceptual spectral plume model for understanding tropical temperature profile and convective updraft velocities. *J. Atmos. Sci.*, **76**, 2801–2814, https://doi.org/10.1175/JAS-D-18-0330.1.